When is flow re-entrainment important for the flushing time in coastal reef systems?

Gundula Winter, B Castelle, R J Lowe, J E Hansen, R Mccall

When is flow re-entrainment important for the flushing time in coastal reef systems?

G. Winter[1], B. Castelle[2], R.J. Lowe[3,4], J.E. Hansen[3,5], R. McCall[1]

[1]Deltares, Dept. ZKS, P.O. Box 177, 2600 MH Delft, The Netherlands.

[2]CNRS, UMR EPOC, University Bordeaux, Pessac, France.

[3]Oceans Graduate School and the UWA Oceans Institute, University of Western Australia, Crawley, Australia.

[4]ARC Centre of Excellence for Coral Reef Studies, University of Western Australia, Crawley, Australia.

[5]School of Earth Sciences, University of Western Australia, Crawley, Australia.

Corresponding author: Gundula Winter (gundulawinter@gmail.com)

Abstract

The rates of water exchange between coastal reef systems and the surrounding ocean are key physical drivers of water quality and reef ecosystems. It is generally assumed that water exiting a reef system through reef channels is predominantly replaced by 'new' water from offshore. However, exiting water may also recirculate back into the reef system reducing the rate of exchange between the reef and the ocean, which has implications for reef water temperatures, nutrient fluxes and population connectivity. To quantify flow re-entrainment at a rocky reef site in southwestern Australia, flow patterns were measured with GPS-tracked drifters during a two-week field experiment. The field observations were extended via a set of idealized numerical experiments to determine the effect of variable oceanic forcing and reef geometry on flow re-entrainment. The observations demonstrate that re-entrainment can vary significantly and the numerical results support the hypothesis that re-entrainment increases with increasing offshore wave height, increasing alongshore currents outside of the reef, and decreasing reef channel spacing but is largely not impacted by reef roughness. Re-entrainment was correlated with a predictor variable R, which is a measure of wave forcing versus the total offshore flow cross-section, and alongshore currents outside the reef. For large values of R and strong alongshore currents, flow re-entrainment increases the effective flushing time by a factor of three or more. The results suggest that flow re-entrainment may be particularly important in small-scale reef systems or reefs exposed to an energetic wave climate and/or strong alongshore currents.

Keywords:

Reef, wave-driven circulation, flushing, Lagrangian, drifter

1 Introduction

The circulation of water within reef systems controls the exchange of dissolved and particulate material between reefs and the surrounding deeper ocean, which substantially influences ecosystems of both tropical coral reefs [see *Lowe and Falter*, 2015 for a review] and temperate rocky reefs [e.g. *Morgan et al.*, 2016]. For example, the influx of water to reefs from the surrounding ocean often has higher nutrient concentrations and is cooler [*Lowe and Falter*, 2015]. As the water flows over shallow reefs, nutrients in various forms are taken up by reef communities at rates influenced by local water motion [*Falter et al.*, 2004]. Furthermore, this influx of water contributes to the regulation of reef water temperatures, which due to the relatively shallow water depths, can either heat or cool relative to the surrounding ocean [*Zhang et al.*, 2013]. Water that exits through the reef channel can also remove suspended sediments [e.g. *Storlazzi et al.*, 2004], larvae [e.g. *Lugo-Fernández et al.*, 2001] as well as pollutants from the reef system (e.g., associated with terrestrial discharge).

Reef circulation can be driven by a combination of different processes including tides [*Black et al.*, 1990], buoyancy differences [*Herdman et al.*, 2015], wind stresses [*Tartinville et al.*, 1997] and breaking waves [*Hoeke et al.*, 2011; *Lowe et al.*, 2009; *Taebi et al.*, 2011]. However, many reef systems that fringe coastlines are exposed to wind (sea-swell) wave energy that provides the main forcing to reef circulation. For these wave-exposed reefs, radiation stress gradients [*Longuet-Higgins*, 1962] that originate from wave dissipation on the forereef or reef crest generate variations in the mean water level over the reef flat and cross-reef currents. In the absence of reef channels (i.e., a one-dimensional, cross-shore system) the setup over a coastal reef is maximum near the shoreline and the net depth-averaged cross-reef mass flux is zero [*Buckley et al.*, 2016; *Vetter et al.*, 2010]. When the reef flat is intersected by reef channels, the net forcing, which is the residual difference between radiation stress and setup gradients, drives a net cross-reef onshore flow that is countered by bed friction

[*Symonds et al.*, 1995]. The return flow in the channel may also be fed directly by alongshore flows entering the channel laterally from the reef platform. The relative contribution of water entering the channel from the lagoon or directly from the reef depends on the relative importance of flow resistance across the reef and along the lagoon, which is governed by the roughness properties as well as geometry of the reef system [*Monismith*, 2013].

In many reef studies, water that exits through a reef channel is assumed to leave the reef system and to be replaced by 'new' offshore water [*Herdman et al.*, 2015; *Lowe et al.*, 2010; *Taebi et al.*, 2011]. While this approach allows ocean-reef exchange rates to be more easily quantified from fixed (Eulerian) measurements, it does not account for water that has initially flowed out through the channel and then returns back into the reef-lagoon system, which will effectively increase the flushing time of the system. While water exchange and flow re-entrainment in wave-dominated reefs have been previously estimated from numerical simulations, these have typically been done for either a specific reef system [e.g. *Zhang et al.*, 2013] or for cases where the wave forcing was not modeled explicitly [e.g. *Herdman*, 2012]. Thus, a systematic approach to flow re-entrainment in wave-dominated reef environments that incorporates the impact of different oceanic forcing and reef geometry is currently lacking and motivates the present study.

The aim of this manuscript is to identify the parameters that govern flow re-entrainment in wave-dominated coastal reef systems. To assess the hydrodynamic response to different parameters, we validate the numerical model XBeach [*Roelvink et al.*, 2009] with field observations from moored instruments and Lagrangian drifters in a coastal reef system. The model is then extended to test the effects of wave forcing and along-shelf currents as well as geometric parameters on flow re-entrainment in an idealized wave-dominated reef system. The specific objectives of this study are to: (i) investigate the variability of flow re-entrainment, (ii) identify the governing parameters that drive this variability and (iii) to assess

the implications of variable flow re-entrainment on flushing time estimates for coastal reef systems, more generally. The results can thus help to classify coastal reef systems as being predominantly open or closed systems [*Cowen et al.*, 2000] based on their specific geometrical characteristics and predominant forcing.

Section 2 provides background on water exchange processes between the nearshore and the open ocean and explains different methods to quantify these exchange processes. Section 3 describes the field experiment and observations. In section 4 we present a numerical model of the field site that has been used to test the sensitivity of flow re-entrainment to variable hydrodynamic forcing and reef geometry in a simplified reef system. Section 5 discusses the physical processes that change with the tested parameters and the impact of the re-entrainment rate on flushing time estimates.

2 Background: Quantifying water exchange rates

Water exchange between a coastal basin (e.g., an estuary or lagoon) and the surrounding open ocean is typically quantified in terms of a flushing time. This time scale is often estimated as the average time (T_f) it takes for the entire volume (V) of water inside the basin to be replaced by 'new' water and can be estimated as [*Fischer et al.*, 1979]:

$$T_f = \frac{V}{Q} \tag{1}$$

where Q is the flux of water into the basin. Importantly, Eq. (1) assumes that the outflow from an enclosed water body is not re-entrained once it exits the basin through defined boundaries [*Monsen et al.*, 2002].

For tidally-flushed systems, Eq. (1) has been extended to include a re-entrainment fraction b that accounts for water that exits the basin and subsequently re-enters the system at a later time [*Sanford et al.*, 1992]:

$$T_f = \frac{V}{(1-b)Q} \quad (2)$$

In prior studies of reef systems, re-entrainment is usually assumed to be zero (b = 0 in Eq. (2)) [*Coronado et al.*, 2007; *Kench*, 1998; *Kraines et al.*, 1999; *Lowe et al.*, 2010; *Taebi et al.*, 2011]. Such a flushing time will therefore represent the minimum time for flushing to occur. However, *Herdman* [2012] found re-entrainment rates in a large-scale tropical coral reef system in Moorea (Polynesia), where circulation is driven by buoyancy and waves, to be 23-50% suggesting that re-entrainment would substantially increase the true flushing time.

Accurate estimates of b in Eq. (2) can be difficult to obtain in the field because flow re-entrainment can only be directly measured in a Lagrangian reference frame where flow pathways are tracked. To overcome this, it is common to evaluate re-entrainment using Lagrangian approaches (such as GPS-tracked drifters or dye), which has been frequently applied in the study of rip currents along beaches [*Austin et al.*, 2010; *Brown et al.*, 2015; *Hally-Rosendahl et al.*, 2014; *MacMahan et al.*, 2010b; *R Jak McCarroll et al.*, 2018; *Reniers et al.*, 2009; *Spydell et al.*, 2007]. These sandy beach environments are often characterized by having shore-parallel sand bars, over which water moves shoreward, and defined channels, through which water returns seaward [*Castelle et al.*, 2016; *Dalrymple et al.*, 2011]. In these studies, the cross-shore exchange has typically been expressed in terms of an exit rate (or its opposite property, the retention rate). This exit (or retention) rate is defined by the number of drifters leaving (or remaining within) the surf zone indefinitely, relative to the total number of drifters initially seeded [*Reniers et al.*, 2009]. Thus, drifters that recirculate and ultimately remain inside the surf zone are accounted for in this definition. In beach environments, the exit rate has been found to correlate with the so-called ‘exit parameter’, which is a function of the surf zone width and the incident wave forcing [*Reniers et al.*, 2009]. This exit rate can be enhanced by geomorphic features such as headlands [*Castelle and Coco*, 2013; *R. Jak*

McCarroll et al., 2014] and by intermittendly spaced rip channels and rip head shoals [*Castelle et al.*, 2014], but can be reduced due to the presence of alongshore currents and obliquely incident waves [*Spydell*, 2016; *Winter et al.*, 2014].

While the nearshore circulation patterns of barred beaches have some analogies to the flows in fringing reef systems, there can be a number of key differences, for example: (1) reef systems can have much larger spatial scales [see *Falter et al.*, 2013], so that the impact of parameters that describe the reef geometry, such as channel spacing, may differ; (2) bed roughness over reefs [*Reidenbach et al.*, 2006] as well as bathymetry gradients are often much greater than over sandy bottoms; and (3) incident waves break on a forereef, which has typically a steeper slope than a sandy beach, so that the width of the surf zone can be much narrower and less variable [*Symonds et al.*, 1982]. It remains unclear how these differences will affect ocean-reef water exchange rates.

3 Field Experiment

3.1 Site description

A two-week field study was conducted during the austral winter (May-June) of 2014 along a 600 m stretch of Garden Island in southwestern Australia (Figure 1a). The beach is fronted by several ~1 m deep limestone reefs, which is typical for much of the southwest coast of Australia. A shore-attached reef platform is located near the center of the site and is flanked to the south by another reef and by a deeper (2-3 m) lagoon (Figure 1c). To the north this group of reef platforms is bounded by a channel and to the south by a more pronounced and deeper channel, which is orientated in a southwesterly direction. The bathymetry of the region was surveyed in 2009 using aerial bathymetric LiDAR with 5 m horizontal resolution and ±0.45 m uncertainty in the vertical [*Department of Transport Western Australia*, 2009]. In addition, a detailed bathymetric survey was conducted during the experiment using a

156 single beam echosounder and RTK-GPS system by small boat and a backpack mounted
157 RTK-GPS system near the shoreline with an estimated uncertainty in the vertical of 0.1 m for
158 surveys by boat [*MacMahan*, 2001] and 0.05 m by foot, respectively [*Barnard et al.*, 2012].
159 The dimensions of the reef platforms and the lagoon are typical of many rocky coastlines as
160 well as many nearshore fringing coral reefs, but smaller than those of some previously
161 studied coral reef systems [e.g. *Herdman*, 2012; *Zhang et al.*, 2012]. The effect of reef scale
162 on flow re-entrainment is discussed in section 5.1.3.

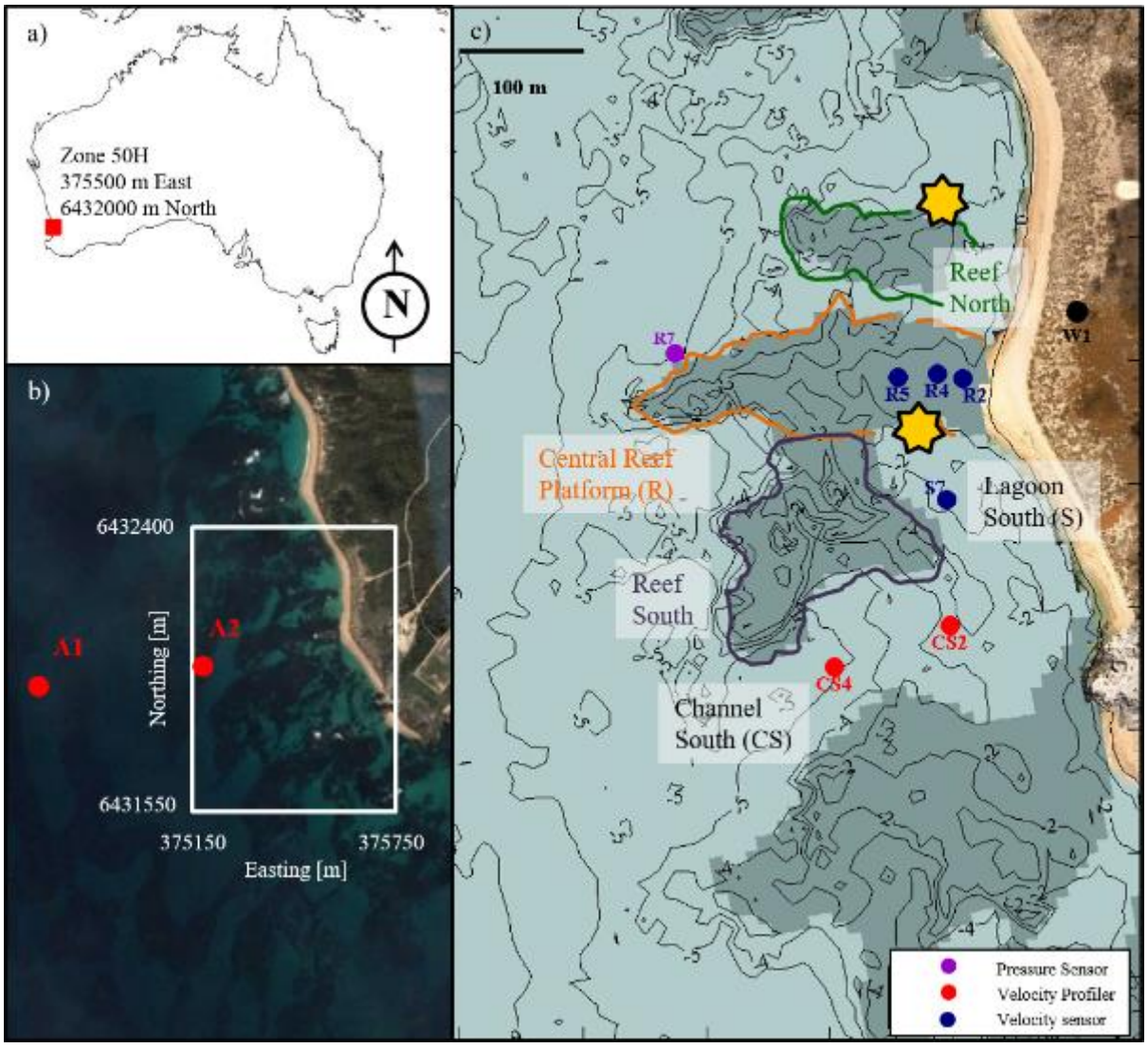

Figure 1. a) Location of the Garden Island study site within southwestern Australia, b) aerial image (Google Earth) of the field site and the locations of the Acoustic Wave and Current meters (AWAC) A1 and A2, c) locations of velocity profilers (red dots), velocimeters (blue

dots) and the anemometer (black dot) as well as drifter release locations in the southern and northern channel (stars). Dark shaded areas in c) indicate submerged reef structures.

The southwest coast of Australia is a micro-tidal environment and during the field experiment the tidal range was between 0.3 and 0.6 m so that tidally induced currents are negligible. Alongshore currents outside the reef on the inner continental shelf (depth up to 20 m) are predominantly driven by a balance between local wind stresses and regional alongshore pressure gradients [*Zaker et al.*, 2007]. The currents can become particularly strong (up to 0.3 m s^{-1}) during the summer months due to persistent southwesterly winds [*Gersbach et al.*, 1999]. Episodic fluctuations in the shelf-scale pressure gradients due to coastally trapped waves and eddies can enhance the variability, and episodically reverse the along- and cross-shore currents on the inner shelf [*Ruiz-Montoya and Lowe*, 2014]. Section 5.1.2 discusses the impact of variable alongshore currents on flow re-entrainment. The southwest coast of Australia receives the highest wave energy events in the austral winter months from May to September *[Bosserelle et al., 2012]* in the period that the experiment took place.

3.2 Instrument Layout

Surf zone exit and re-entrainment rates were quantified using Lagrangian drifters, similar to the design by *Schmidt et al.* [2003], over 8 days during the experiment. When floating freely, all but the uppermost ~5 cm of the drifter bodies were submerged. Based on a similar drifter design, wind drift was estimated at 1% of the wind speed measured 0.5 m above the water surface [*Schmidt et al.*, 2003] and therefore is not expected to affect the drifters during this experiment (expected drift due to windage < 0.05 ms^{-1}). Drifter positions were recorded at 10 Hz by a Qstarz BT-Q1000eX GPS logger placed in the top of each drifter. For each of the 8 deployment days, 12 to 15 drifters were released for two to four hours at a time (Table 1). Drifters were deployed in clusters, mostly inside the southern

lagoon (8 of the 11 deployments), with the remaining deployments inshore of the northern channel (yellow stars in Figure 1c). This manuscript focuses primarily on the deployments in the southern lagoon because the lagoon connects to the better defined southern channel. During each deployment, any drifters that beached or exited the reef-system were retrieved and redeployed at the initial release location. Data recorded by the GPS loggers were initially averaged in 1 Hz blocks to remove noise. Short wave motions were then removed by applying a moving average filter of 25 s so that only infragravity and slowly varying mean current motions were preserved in the recorded drifter tracks. The low-pass filtered positions were numerically-differentiated to determine the velocities of the drifters. The velocity and vorticity of all drifter observations was averaged over cells of 20 m by 20 m.

Table 1. Drifter deployments: Number of drifters deployed on each day, total duration of each drifter deployment, offshore wave conditions, observed return flow regime (only in the southern channel) and deployment location.

Day	Number of drifters	Duration (hours)	H_{m0} [m]	T_p [s]	θ_p [ºN]	Water depth on the reef [m]	Along-shelf current [m s^{-1}]	Return flow regime in the southern channel	Deployment location
1	12	3:40	1.66	14	266	1.00	0.04	Re-entrainment	Southern lagoon
2	15	4:24	1.49	13	265	0.99	0.05	Re-entrainment	Southern lagoon
3	15	2:28	1.48	14	262	0.96	-0.02	Combination	Southern lagoon and northern channel
4	15	1:46	1.24	14	268	1.21	-0.06	Exiting	Southern lagoon
5	15	2:56	1.31	13	261	1.21	-0.1	Exiting	Southern lagoon and northern channel
6	15	3:58	1.13	12	261	1.11	-0.05	Re-entrainment	Southern lagoon
7	15	3:22	1.24	18	267	1.09	-0.05	Exiting	Southern lagoon
8	14	2:47	1.40	15	266	1.06	-0.02	Re-entrainment	Southern lagoon and

									northern channel

196 In addition to the drifters, acoustic Doppler velocimeters and profilers measured
197 velocities and wave conditions throughout the experiment at six sites within the reef-lagoon
198 system (Table 2 and Figure 1c). For instruments in the shallow reef-lagoon system (depths <5
199 m), the velocities were low-pass filtered to remove fluctuations shorter than 15 minutes, and
200 in the case of the velocity profilers, the velocities were depth-averaged. On the inner shelf
201 (site A1 in 11 m water depth, Figure 1b), an Acoustic Wave and Current meter (AWAC)
202 recorded offshore waves and currents. Drifter deployments were conducted at similar tidal
203 water levels of 0.25 m above Australian Height Datum (AHD, approximately mean sea level)
204 during falling tide (Figure 2a). During the deployments the incident significant wave heights
205 at A1 ranged from H_{m0} = 1.0–1.8 m, peak periods from 12–18 s and directions from 260–270º
206 (Figure 2b–d). At sites A1 and A2 the hourly mean velocities were averaged over the
207 uppermost 1.5 m of the water column, where they were usually strongest. At site A1, the
208 surface currents varied between -0.1 m s^{-1} and 0.05 m s^{-1} during the deployments (Figure 2e).

Table 2. Instruments and sampling configuration. "A" denotes offshore instruments, "CS" instruments in the southern respectively, "R" instrument on the reef platform and "S" south of it.

Site	Instrument	Depth	Sampling configurations	H_{m0} (RMSE, bias, WS)	u (RMSE, bias, WS)	v (RMSE, bias, WS)
Offshore						
A1	Nortek AWAC	10.5 m	Pressure and surface velocities in hourly bursts of 2048 s at 2 Hz, velocity profile hourly in 0.5 m bins			
Within the reef-lagoon system						
CS2	Nortek ADP High Resolution (HR)	3.1 m	Pressure and velocity profile at 1 Hz continuous in 0.05 m bins	0.42 m, 0.42 m, 0.58	0.02 m s^{-1}, 0.00 m s^{-1}, 0.95	0.11 m s^{-1}, -0.11 m s^{-1}, 0.86
CS4	RDI ADCP	5.4 m	Pressure and velocity profile at 1	0.35 m, 0.35 m, 0.64	0.06 m s^{-1}, 0.05 m s^{-1}, 0.90	0.11 m s^{-1}, -0.11 m s^{-1}, 0.88

			Hz continuous in 0.1 m bins			
R2	Nortek ADV	1.2 m	2 Hz continuous	0.08 m, -0.07 m, 0.91	0.08 m s^{-1}, -0.07 m s^{-1}, 0.90	0.09 m s^{-1}, 0.08 m s^{-1}, 0.90
R4	Nortek ADV	1.0 m	2 Hz continuous	0.04 m, -0.02 m, 0.97	0.12 m s^{-1}, -0.10 m s^{-1}, 0.84	0.13 m s^{-1}, 0.12 m s^{-1}, 0.85
R5	Nortek ADV	1.2 m	2 Hz continuous	0.09 m, -0.09 m, 0.91	0.13 m s^{-1} -0.07 m s^{-1} 0.78	0.12 m s^{-1}, 0.10 m s^{-1}, 0.86
R7	RBR Virtuoso	5.2 m	1 Hz continuous	0.13 m, 0.11 m, 0.92	-	-
S7	Nortek ADV	2.3 m	2 Hz continuous	0.13 m, 0.12 m, 0.82	0.05 m s^{-1}, 0.05 m s^{-1}, 0.93	0.05 m s^{-1}, -0.03 m s^{-1}, 0.95
On land						
W1	Young Ultrasonic Anemometer 85106	10 s average				

209

210 Wind was measured on the dune near the salient with an ultrasonic anemometer
211 (Young 85106) that sampled average wind speeds at 10 s intervals. This anemometer did not
212 sample continuously due to power interruptions and missing data were filled in by wind
213 speeds and directions sampled half-hourly 700 m inland from the field site [*Bureau of*
214 *Meterology Commonwealth of Australia*, 2014]. In the overlapping periods, the locally
215 measured wind data correlated well with the inland measurements (R^2 = 0.90 and R^2 = 0.94
216 for cross-shore and alongshore wind speeds, respectively). During the deployments, wind
217 speeds varied between 2–5 m s^{-1} and came from a range of directions (Figure 2f).

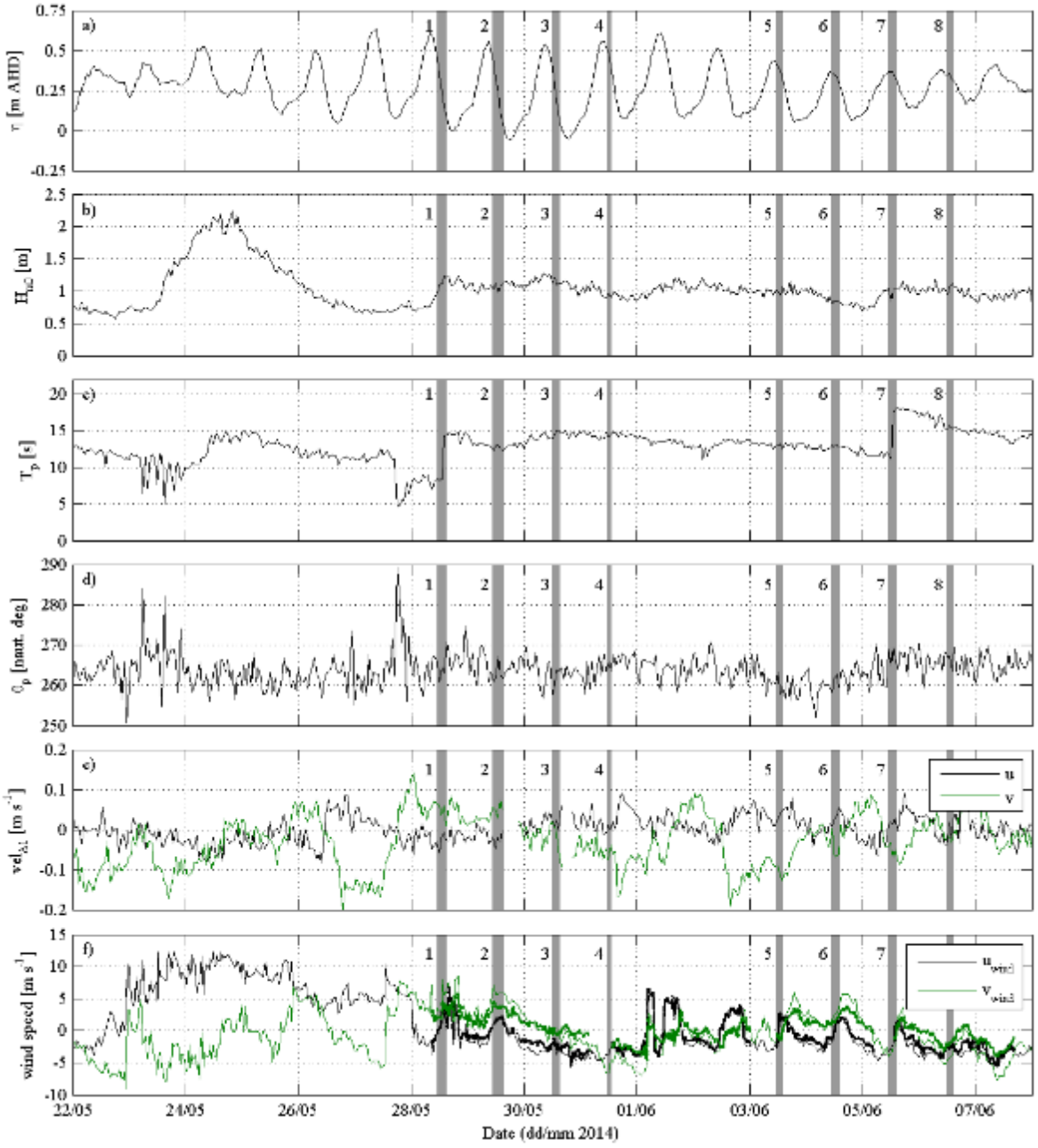

218 Figure 2. Site A1: a) Tidal water level relative to AHD, b) significant wave height at, c) peak
219 wave period at A1, d) peak wave direction at A1, e) cross- and alongshore currents in the
220 most upper 1 m of the water column at A1. Site W1: f) cross-shore and alongshore wind
221 speed measured at W1 (thick lines) and by the *Bureau of Meterology Commonwealth of*
222 *Australia* [2014] (thin lines). Positive cross-shore (*u*) and alongshore (*v*) velocities are
223 directed shoreward and northward, respectively. Grey shaded areas denote the times of drifter
224 releases and the numbers from 1 to 8 denote the day of drifter deployment. See Figure 1 for

the locations of sites A1 and W1.

3.3 Quantifying re-entrainment

To provide a quantitative measure of flow re-entrainment, we evaluated the exchange rate between lagoon and ocean waters using two different definitions of the exit rate, based on either excluding or including the effect of re-entrainment. Both these exit rates were calculated for the drifters deployed in the field as well as those simulated in the numerical model XBeach (Section 4). The first exit rate E_1 is based on the commonly used minimum flushing time described by Eq. (1) and is defined as the ratio of the number of drifters that leave the reef-lagoon system in seaward direction (L) and the total number of drifters initially seeded (N), i.e.

$$E_1 = \frac{L}{N} \tag{3}$$

The offshore boundary of the reef-lagoon system is defined as the cross-shore position where the alongshore-averaged roller energy (as calculated in XBeach) exceeded 10% of the maximum roller dissipation in accordance with studies on rip-channeled beaches [e.g. *Reniers et al.*, 2009].

The second exit rate definition (E_2) accounts for re-entrainment and thus corresponds to a more realistic estimate of the amount of flushing. The exit rate E_2 is defined as the ratio of drifters retrieved outside the reef-lagoon system at the end of the deployment over the total number of drifters released within the reef system (N). The total number of drifters outside the reef-lagoon system is the difference between the number of drifters that left the lagoon seaward through the channel (L) and the number of drifters that return back to the reef-lagoon system (B):

$$E_2 = \frac{L - B}{N} \tag{4}$$

This definition is similar to the definition used in surf zone exchange studies on beaches [*MacMahan et al.*, 2010a]. When the drifters were released, the number of drifters outside the reef-lagoon system (E_2) typically increased and then fluctuated around a constant value (see, for example, Figure 4, Day 1 and 6). These fluctuations were related to groups of drifters simultaneously exiting and re-entering the lagoon. We note that this exit rate definition E_2 does not distinguish between re-entrained drifters and drifters that remained inside the reef-lagoon system, i.e. there is no difference between low exchange rates due to stagnant flow and due to energetic recirculating flow [similar to the residence time approach in *Zhang et al.*, 2012]. E_2 is thus not a suitable measure to quantify the return flow regime of water that exits the channel.

A parameter that specifically describes the return flow regime is the flow re-entrainment b (Eq. (2)), which is defined as the number of drifters re-entering the lagoon (B) divided by the number of drifters that have exited the channel (L), and was quantified by combining Eqs. (3) and (4):

$$b = \frac{B}{L} = \frac{E_1 - E_2}{E_1} \tag{5}$$

We note that water exiting the channel may be mixed with the surrounding ocean water through lateral dispersion and that b may also be smaller than estimated from Lagrangian drifter measurements or simulations. Numerical modelling indicates that sub-grid mixing using the *Smagorinsky* [1963] model accounted for less than 5% in the momentum balance equation and was negligible. Hence, advection is the dominant process to transport material offshore or to re-entrain it back into the reef-lagoon system.

3.4 Field Observations

The drifter pathways displayed two main patterns over the course of the study: (i) complete drifter re-entrainment (Figure 3a and b), (ii) complete drifter ejection offshore (Figure 3c and d), and a combination of pattern (i) and (ii).

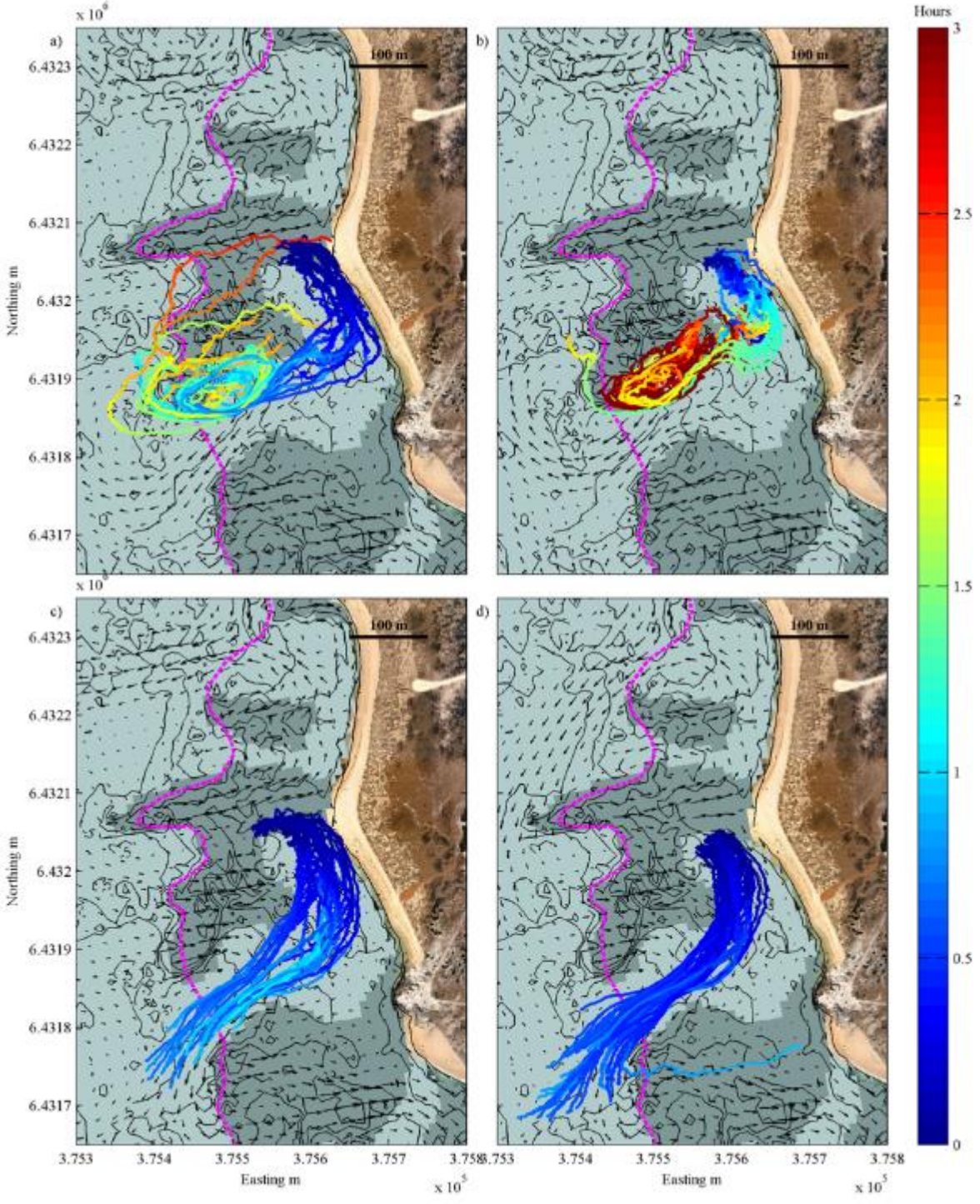

Figure 3. Examples of observed drifter trajectories that become re-entrained on a) Day 1 and

b) Day 2 and drifters that exit the reef system on c) Day 5 and d) Day 7. The colors indicate time in hours since individual drifter deployment and the vectors are mean velocities obtained from the model. The pink line marks the outer edge of the surf zone defined as the cross-shore position where the roller energy exceeds 10%, which was derived from the XBeach results. The surf zone has been interpolated across the channels where no wave breaking occurred.

In flow pattern (i), drifters released in the southern lagoon drifted southward parallel to the shore, turned sharply seaward in the middle of the embayment and then floated offshore along the edge of the channel. Most of the drifters turned north outside the channel and re-entered over the reef in a tight circulation cell. In flow pattern (ii), drifters floated seaward along the center of the channel and exited in a southwesterly direction. Drifters typically left the reef system within an hour or less after their deployment inside the southern lagoon (see colors in Figure 3c and d). In contrast, re-entrained drifters remained within the reef lagoon system for two hours or more (see colors in Figure 3a and b). We classified the eight drifter deployments into predominantly exit or re-entrainment flow patterns. Day 1, 2, 3, 6 and 8 were characterized by (partial) drifter re-entrainment. Initially, all drifters were seeded inside the reef-lagoon system (green areas, Figure 4). Drifters then exited the reef system (yellow) and re-entered so that at any point in time a proportion of drifters was inside and the remaining drifters were outside the reef-lagoon system. On Day 1, drifters circulated in a wide eddy so that at any given time E_2 ~ 50% of all drifters were offshore of the breaker zone (Figure 4). All of these drifters re-entered the lagoon and the re-entrainment rate b was 100%. On Day 2, drifters remained mostly onshore of the breaker line and thus E_2 was low (10%). Drifters were retrieved gradually inside the lagoon after circulating numerous times, hence the gradual decrease of total drifters. On Day 3, a large number of drifters (E_2 = 76%) exited the reef-lagoon system indefinitely and only a small number of drifters (b = 26%)

290 recirculated. Similarly, on Day 6 only 46% of the drifters were re-entrained. Exiting drifters
291 were retrieved and redeployed again inside the lagoon so that the total number of drifters
292 floating freely fluctuated. On Day 4, 5 and 7, all drifters exited the reef system, were
293 retrieved offshore and re-deployed all at once within the lagoon. On Day 8, part of the drifters
294 left the reef system, mostly re-entered the lagoon and were retrieved both outside and inside
295 the reef-lagoon system.

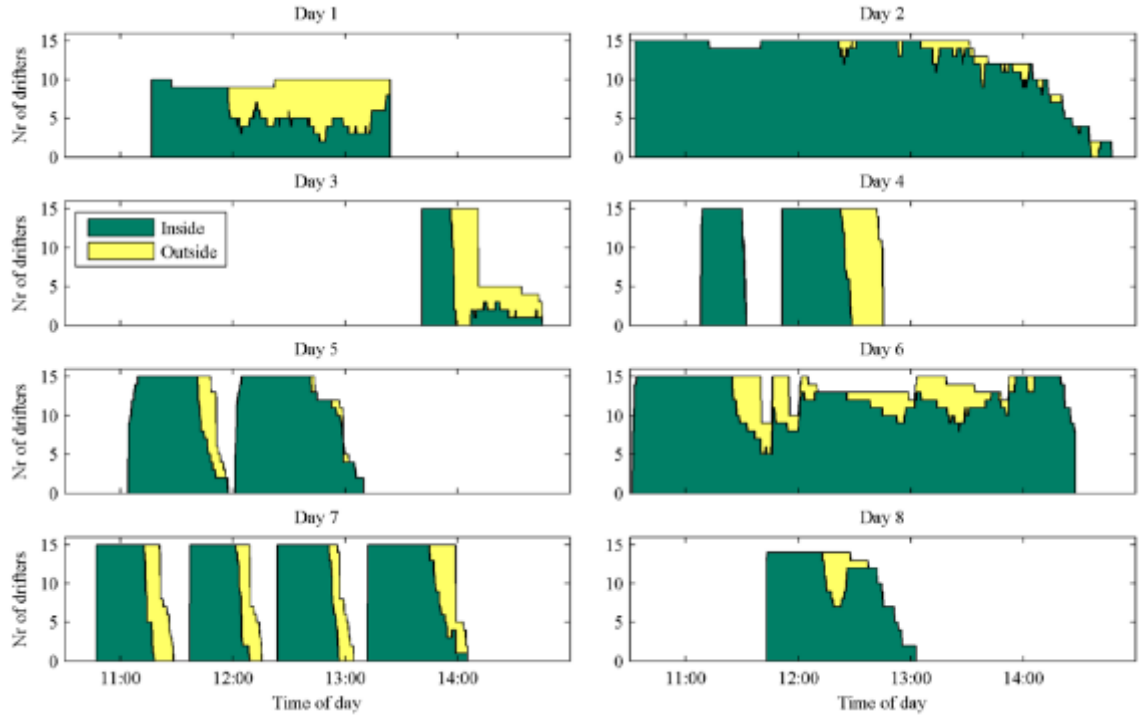

Figure 4. Number of drifters inside (green) and outside (yellow) the reef-lagoon system as a function of time for each day. Day 1, 2, 3, 6 and 8 were characterized by (partial) drifter re-entrainment and Day 4, 5 and 7 by drifter exits.

296

297 In general, drifters were more likely to re-enter the lagoon when they floated
298 alongside the channel edge where they were caught in an eddy (marked by the high vorticity
299 in Figure 5a) than when they floated along the center of the channel in a south-westerly
300 direction (Figure 5b). The re-entrainment pattern was dominant when wave heights were
301 large, water levels were low and alongshore velocities were directed northward and thus

302 favoring drifters returning over the reef to the north of the southern channel (Table 1).

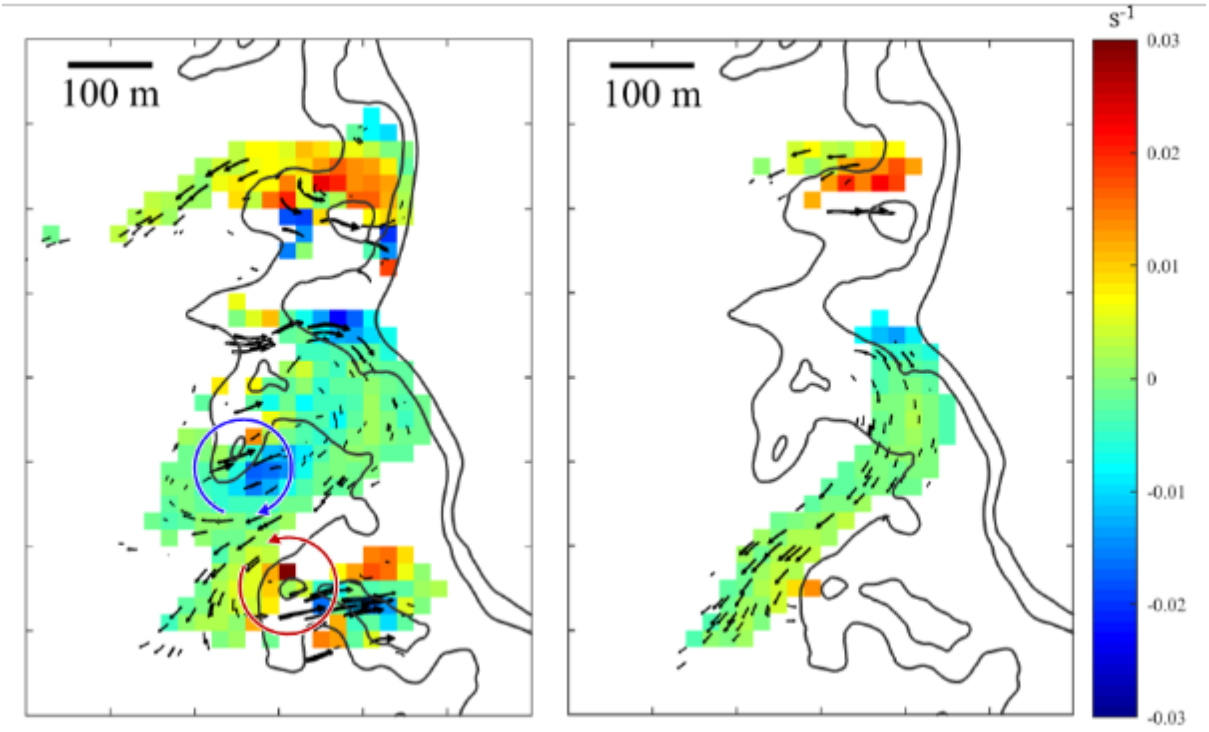

Figure 5. Drifter velocity (black arrows) and vorticity (colours) averaged over all drifter deployments, in which retention dominated (left) and in which exits dominated (right) interpolated on a 20 m x 20 m grid. Red (blue) circles in the left panel indicate eddies rotating in clockwise (anti-clockwise) direction. In the right panel, information on drifter velocity is mostly absent along the channel edges because drifters generally floated along the centre of the channel in exit dominated flow regimes.

303

304 The qualitative observations of drifter behavior and flow patterns over the course of
305 the field experiment motivated a numerical sensitivity study of re-entrainment in an idealized
306 reef to understand and predict the response to varying wave height, alongshore current and
307 variable reef geometry (section 4.3).

4 Numerical Model

4.1 Model description

The general influence of reef geometry parameters and offshore hydrodynamic conditions on water exchange rates were further investigated using the numerical model XBeach configured in a short wave-group (surf beat) mode (refer to *Roelvink et al.* [2009] for details of the model). This model couples a module describing the wave-group varying wave energy with a non-linear shallow water wave module to describe wave-averaged flow, including wave setup, infragravity waves and wave-current interactions, and has been successfully used in other two-dimensional reef studies [*van Dongeren et al.*, 2013] as well as numerical experiments on drifter retention on rip channeled beaches [*Castelle et al.*, 2014].

The analysis of the model output was conducted in two stages. Firstly, to gain confidence that the model is capable of accurately reproducing drifter exits and retention, we performed hindcast simulations of the drifter observations based on the bathymetry of the field site at Garden Island. The model was forced by JONSWAP spectra on the offshore boundary (~11 m depth) that represented the significant wave height, peak period, directional and frequency spreading of the frequency-direction variance density spectra measured at the offshore AWAC A1 (Figure 1b). Bathymetry within the model domain was derived from the aerial LiDAR and single beam echosounder surveys. Wave breaking was simulated using the dissipation formulation proposed by *Roelvink* [1993] with $\gamma = 0.7$, which is similar to previous reef hydrodynamic models [*Lowe et al.*, 2010] and provided better results than other values of γ tested in this study within the typical range from 0.5 to 0.7 [*van Dongeren et al.*, 2013]. The wave forcing that generates wave setup and currents within the flow module included radiation stresses due to short waves and wave rollers. Sub-grid turbulence was modelled using the *Smagorinsky* [1963] turbulence closure model. The domain consisted of

190 grid cells in the alongshore by 103 cells in the cross-shore with a resolution of 6 x 6 m in the areas of interest over the reef and in the lagoon. Each simulation was allowed one-hour spin-up time, which was adequate to establish a steady state wave-driven reef circulation, and the subsequent hourly output was used to calculate time-averaged flow and wave quantities. For computational efficiency, the hindcasts were performed for specific one-hour periods each day coinciding to daily maximum and minimum water levels (diurnal high and low tide) as well as intermediate tide stages. This resulted in 64 hindcast simulations (four per day), which were used to assess the model performance for variable wave and water level conditions.

Bottom friction was modeled as [*Feddersen et al.*, 2000; *Ruessink et al.*, 2001]:

$$\tau^b = c_f \rho \sqrt{(1.16 u_{rms})^2 + (u_E + v_E)^2} \quad (6)$$

where τ^b is the bottom friction, c_f is the depth-independent friction coefficient, ρ the water density, u_{rms} the root-mean-squared orbital wave velocity and u_E and v_E are the depth-averaged cross-shore and alongshore velocities. Within the sandy areas (i.e. lagoon, channels and offshore), we assumed that bed friction was comparable to typical values reported at beaches using an equivalent friction formulation [*Feddersen et al.*, 2000] and set the bed friction coefficient to $c_f = 0.003$ [e.g. *Feddersen et al.*, 1998]. Based on initial model testing we calibrated the bed friction over the reef areas (darker shades in Figure 3) to $c_f = 0.01$, which is lower than values reported for coral reefs using an equivalent friction parameterization (values have typically been found to range from 0.009-0.027 over reefs; see Table 1 in *Rosman and Hench* [2011]). This lower friction coefficient is conceivable for a weathered limestone reef with algae cover. Wind stresses were applied in the model based on the measured wind velocities and a quadratic wind drag coefficient of $C_D = 0.002$ [*Large and Pond*, 1981]. However, including wind forcing terms did not affect the model skill even

355 during the storm event, when the wind speed exceeded 12 m s^{-1} because the wind stress terms
356 were an order of magnitude smaller than the dominant wave and pressure forcing terms.
357 Along-shelf currents offshore of the reef were simulated by imposing an alongshore pressure
358 gradient to reproduce the weak, moderate or strong north- or southward directed currents
359 observed in the surface layer at A1.

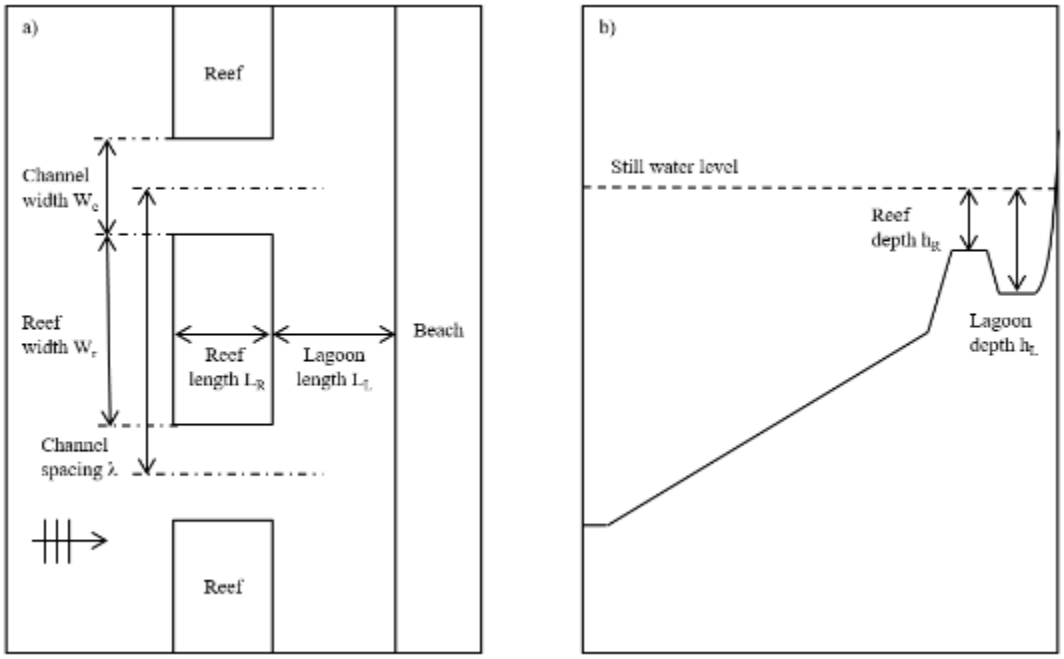

360 Figure **6**. Schematized reef dimensions: a) top view and b) cross-sectional view. The
361 default values for channel width, reef length and depth as well as lagoon length and depth
362 were W_C = 100 m, L_R = 150 m, h_R = 1.5 m, L_{Lag} = 150 m and h_{Lag} = 3 m, respectively.

363

364 In the second stage of the analysis, we simplified the bathymetry to isolate the impact
365 of various hydrodynamic parameters and reef geometries on flow re-entrainment. For this
366 analysis, the bathymetry at Garden Island was schematized with rectangular reefs that were
367 intersected by regularly spaced channels (Figure **6**). This geometry was similar to the reef-
368 fringed lagoon to the south of the platform, where most of the drifters were deployed. In a
369 series of simulations, parameters of the idealized reef system (channel spacing and reef

370 friction) and hydrodynamic forcing (offshore wave height and along-shelf current) were co-
371 varied, while other parameters were kept constant. The model reef was 150 m wide in the
372 cross-shore and was located 150 m from the shoreline. The lagoon and channel were 3 m
373 deep and connected to a beach face with a concave profile $z = Ax^{2/3}$ [*Dean*, 1977; *González*
374 *et al.*, 1999], where x is the cross-shore coordinate, and A was set to 0.15. All simulations
375 were forced at the offshore boundary by waves comprised of a JONSWAP spectrum of
376 normally incident waves with peak period T_p = 14 s (the average observed during the
377 experiment at Garden Island), a peak enhancement factor of $\gamma_{jonswap}$ = 3.3 and a directional
378 spreading of σ = 25°. Simulations with the same wave height were forced by identical time
379 series. After a one-hour spin-up time, 2121 uniformly spaced drifters were seeded as passive
380 particles inside the reef-lagoon system and their tracks were simulated for three hours using
381 Lagrangian particle tracking.

382 The reef parameters (channel spacing and reef friction) and hydrodynamic forcing
383 (offshore wave height and along-shelf current) were varied independently according to Table
384 3, resulting in a total of 320 simulations. The choice of hydrodynamic parameters was
385 motivated by the field observations (see section 3.4) and the reef parameters were chosen
386 based on initial parameter tests and also varied to cover a range of typical fringing reef
387 dimensions with channel spacing from 300 m to 700 m [*Falter et al.*, 2013] and roughness
388 values, which have been previously reported to range from c_f = 0.009 to 0.027 [*Rosman and*
389 *Hench*, 2011].

Table 3. Parameters (see also Figure **6**) and parameter values used in the sensitivity test. Parameter values for the default case are highlighted in bold.

Parameter	Values
Variable	
Channel spacing λ	300, **400**, 500, 600, 700 m
Reef friction $c_{f,R}$	0.003, **0.01**, 0.03, 0.1
Significant offshore wave height H_{m0}	1.0, **1.5**, 2.0, 2.5 m
Alongshelf current	**0**, 0.05, 0.10, 0.15 m s^{-1}

Constant	
Reef length L_R	150 m
Reef depth h_R	1.5 m
Channel width W_C	100 m
Forereef slope m	1:40
Lagoon depth h_{Lag}	3 m

To determine the exit and re-entrainment rates the modelled drifters were first allowed to propagate for an hour through the reef-lagoon system. As drifters exited and re-entered the lagoon in groups, the number of drifters offshore from the reef fluctuated. To eliminate the effect of these fluctuations, the exit rate E_2 was averaged over the last two hours of each simulation. This time was sufficient for drifters to finish at least one circulation cycle even in large lagoons. This approach is similar to the time averaged values used by *Castelle et al.* [2014], *Castelle and Coco* [2013] and *Reniers et al.* [2009].

4.2 Hindcast Model Results

The overall model performance was quantified in terms of the root mean square error (RMSE), bias and the Willmott skill (WS) [*Willmott et al.*, 1985], which are defined as:

$$RMSE = \sum_{i=1}^{N} \sqrt{|X_{mod} - X_{obs}|^2} \tag{7}$$

$$bias = \sum_{i=1}^{N} X_{mod} - X_{obs} \tag{8}$$

$$WS = 1 - \frac{\sum_{i=1}^{N} |X_{mod} - X_{obs}|^2}{\sum_{i=1}^{N} (|X_{mod} - \bar{X}_{obs}| + |X_{obs} - \bar{X}_{obs}|)^2} \tag{9}$$

where X_{mod} and X_{obs} are the modelled and observed values (here sea-swell wave height H_{m0}, u_{mean} and v_{mean}), the overbar indicates time averaging of these values and N is the number of samples (N = 64, four simulations per day).

At sites inside the lagoon (S7), offshore from the reef (R7) and on the reef platform (R2), the wave heights were accurately predicted over the duration of the experiment (RMSE = 0.08 – 0.13 m, bias = -0.07 – 0.12 m and WS = 0.82 – 0.92, Table 2). However, in the channel at CS2 and CS4 the model overestimated wave heights consistently by 20%. This may be due to visually observed bathymetric features inside the channel, which are smaller than the resolution of the LiDAR bathymetry (~5 m), and thus not resolved in the model. Further, wave diffraction may play a role at this site, which is not in the model. The alongshore velocities in the channel at CS2 and CS4 were consistently overestimated by ~0.1 m s^{-1} but followed the trends in the observations well. This resulted in a flow that was directed slightly more alongshore in the model, despite the total velocity magnitude being predicted well (not shown). Overall, the RMSE for the modelled velocities ranged between 0.05 and 0.13 m s^{-1}, the bias between -0.11 and 0.12 m s^{-1} and the WS was between 0.78 and 0.95 (Table 2).

The model results were predominantly compared spatially to the observed drifter tracks as for the objectives of this study the spatial patterns were most important. The model produced a circulation cell to the north of the channel, which is in agreement with the observed drifter re-entrainment (Figure 3a, b). However, the modelled re-entrainment cell had a somewhat wider radius than in the field observations, which is most likely due to the combination of bathymetry and model resolution not being able to capture the very steep bed level gradient from the channel to the reef resulting in a more alongshore directed flow. The model also reproduced the southwesterly trajectory of flow exiting the southern channel (Figure 3c, d). Overall, the model was able to replicate the flow magnitudes, directions and patterns with reasonable accuracy and was able to qualitatively reproduce the observed flow patterns.

4.3 Effect of hydrodynamic and reef geometry parameters

The primary goal of the numerical model was to identify the parameters and mechanisms that control flow re-entrainment. For each simulation with varying reef geometry and hydrodynamic forcing the exit rates E_1 and E_2 (Eq. (3) and (4), respectively) and re-entrainment b (Eq. (5)) were calculated. The mean offshore and onshore velocity across all reef channels and reef structures, respectively, were determined at the cross-shore location where the offshore current in the channel was maximum. This location was typically just offshore from the channel exit.

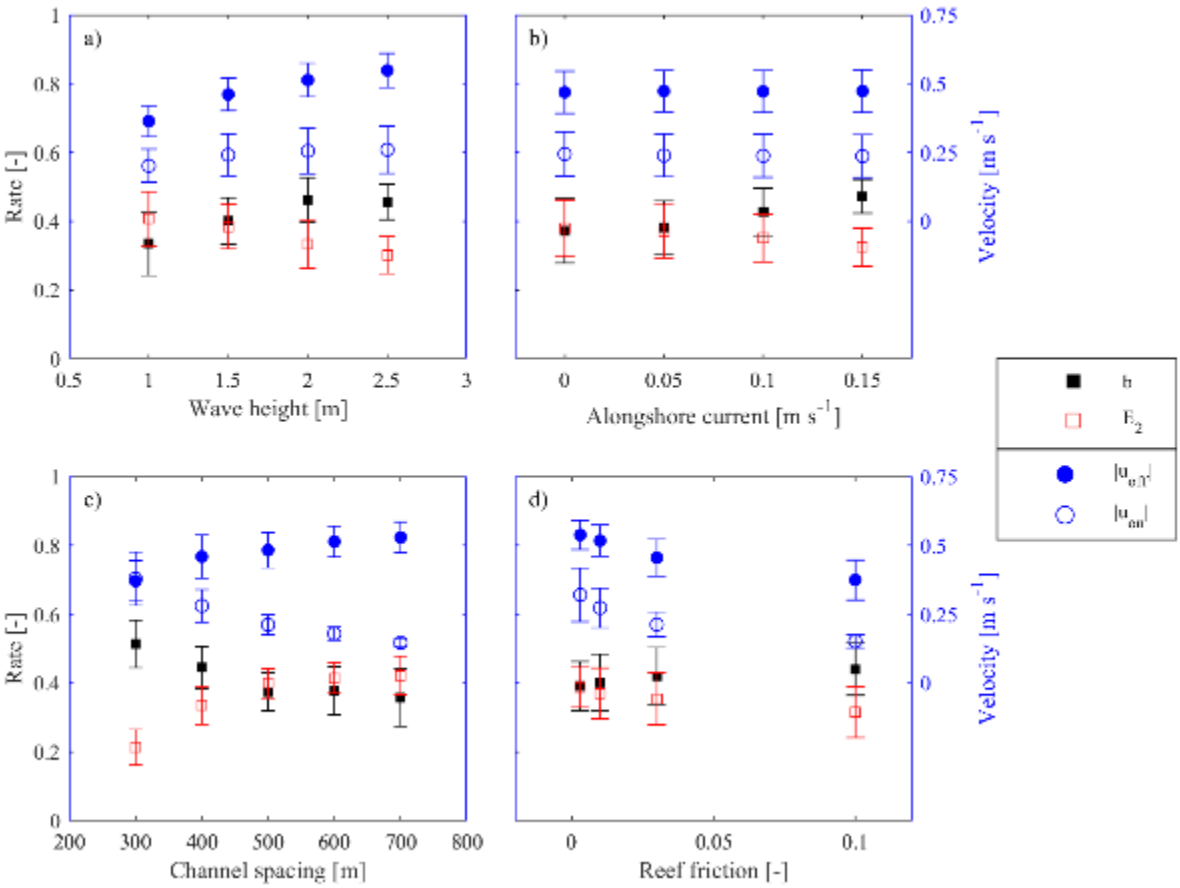

Figure 7. Re-entrainment b, exit rate E_2, average offshore velocity in the channel and average onshore velocity at the reef edge as functions of variations in a) wave height, b) alongshore current outside the reef, c) channel spacing and d) lagoon length. The circle marks the mean value of all simulations and the black bar indicates the range in which 50% of the simulation

results fall within.

436

437 The drifter re-entrainment *b* increased (exit rate E_2 decreased) with increasing wave
438 height (Figure 7a) and increasing alongshore current outside the reef (Figure 7b). Large
439 waves caused the maximum offshore flow velocity in the channel and the onshore flow
440 velocity over the reef to increase (Figure 7a) while the alongshore velocity outside the reef
441 had no impact on the cross-shore velocities (Figure 7b). With large channel spacing re-
442 entrainment *b* decreased (exit rate E_2 increased) while the onshore velocities decreased and
443 the offshore velocities increased (Figure 7c). Large bed roughness is a characteristic feature
444 of many (or most) reefs that distinguishes these systems from analogous rip-channeled beach
445 environments. Large reef friction equally reduced the onshore velocities over the reef and the
446 offshore velocities in the channel. Drifters were thus neither more likely to exit offshore nor
447 to return onshore over the reef and the re-entrainment of the drifters remained unchanged
448 (Figure 7d).

449 **5 Discussion**

450 The dynamics of wave-driven flows in reef environments and ocean-reef exchange
451 have been either studied in a Eulerian reference frame that quantifies the incoming water flux
452 across the reef platform and the offshore flux exiting the reef channels [e.g. *Hench et al.*,
453 2008; *Hoeke et al.*, 2011; *Lowe et al.*, 2009; *Taebi et al.*, 2011] or by tracking simulated
454 particles [*Zhang et al.*, 2012]. These approaches have not allowed to identify the governing
455 drivers of reef exchange processes. For estuarine exchange processes, the drivers of
456 recirculation have been identified to be tidal residual currents and baroclinically driven
457 currents *[see Geyer and MacCready, 2014, for a review]*. This study provides insight into the
458 processes related to reef geometry and forcing conditions that control the proportion of water

459 that recirculated in a reef system.

460 Field observations suggest that re-entrainment can vary substantially due to variations
461 in hydrodynamic forcing conditions alone (incident wave heights and along-shelf currents).
462 This is consistent with the numerical model that assessed the effect of a range of reef
463 geometries along with a larger range of variable hydrodynamic conditions, so that re-
464 entrainment varied between 7% and 73%. Importantly, these results demonstrate that the
465 definition of the exit rate E_1 (Eq. (3)), which ignores the effect of re-entrainment and counts
466 all drifters that flow seaward through the channel as exiting, was consistently higher over the
467 range of tested parameters. This definition is analogous to flushing time estimates commonly
468 used with Eulerian velocity measurements obtained using fixed (moored) instruments [e.g.
469 *Taebi et al.*, 2011]. Our results suggest that flushing time estimates purely based on the
470 offshore velocity are not always representative because they discount the effect of flow re-
471 entrainment. In the following, we investigate the effect of a number of hydrodynamic and
472 geometric parameters on reef re-entrainment to determine the conditions and environments in
473 which flow re-entrainment is an important process to consider.

474 5.1 Influence of hydrodynamic and reef geometry parameters on flow dynamics

475 To further investigate how the physical mechanisms responsible for re-entrainment
476 are controlled by reef geometry parameters and hydrodynamic forcing conditions, we first
477 assessed the momentum balances (Appendix A) across the reef-lagoon system for the default
478 simulation that was forced with 1.5 m waves. The channels were spaced 400 m apart and no
479 alongshore current was imposed outside the reef (Table 3). In this case, 71% (E_1) of all
480 seeded drifters floated offshore through the channel and 43% (E_2) remained outside of the
481 reef-lagoon system. Of the drifters that floated offshore 40% (b) were re-entrained back into
482 the reef system. The wave forcing induced by wave breaking on the forereef and the reef

platform (Figure 8a) was balanced mostly by cross-shore pressure gradients (Figure 8b, see also, e.g. *Symonds et al.*, 1995; *Taebi et al.*, 2012). The net forcing, which we refer to as the sum of the offshore directed pressure gradient and onshore directed wave forcing, is directed onshore over the reef platform (Figure 8c), where it drives the cross-reef current that contributes to a relevant bottom shear stress over shallow and rough reefs (Figure 8e). Near the channels, the net forcing is balanced by advection (Figure 8d) and generates counter-rotating eddies (Figure 8f) that, together with the onshore flow over the reef, were responsible for re-entrainment (see also Figure 5). The following sections assess how this momentum balance changes, particularly the strength of the net forcing term, when hydrodynamic forcing or reef geometry are altered.

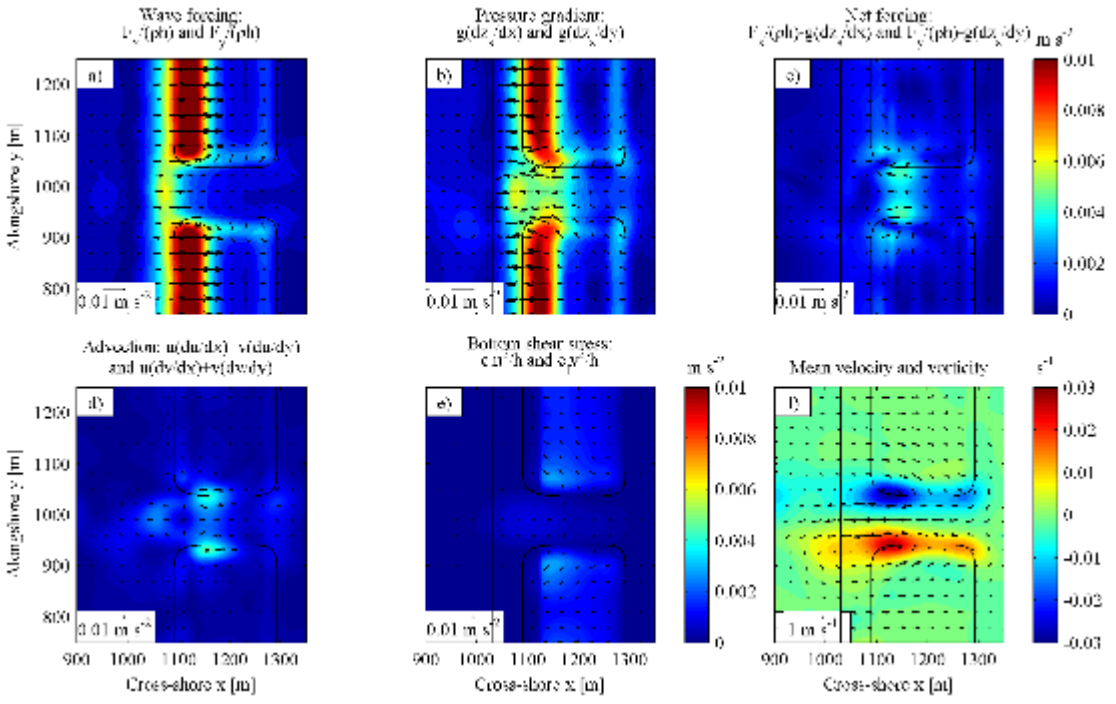

Figure 8. Simulated magnitude and direction of the momentum terms (cross- and alongshore, see Eq. A1-2) for the default case. From top left to bottom right, the contributions from: a) wave forcing, b) pressure gradient, c) sum of wave forcing and pressure gradient, d) non-linear advection, e) bottom shear stress and f) mean velocity with Stokes drift (vectors) and vorticity (colors). Viscosity terms were negligible and are not shown. Black contour lines indicate the -2.5 m and -1 m isobaths. For clarity only every third vector is shown in cross-

and alongshore direction.

5.1.1 Wave height

In both the field observations and the numerical model, the re-entrainment increased with larger offshore wave heights. Larger waves strengthen the net forcing responsible for the wave-driven flows (i.e., the difference between the wave forcing and pressure gradient) just offshore from the reef (x = 1050m, Figure 9a) and on the parts of the reef near the channel from where the offshore flow is primarily fed [*Svendsen et al.*, 2000]. This net forcing drives a stronger onshore flow just outside the reef and a stronger offshore flow in the channel (Figure 7a), which also enhances the strength of the channel vortices (Figure 9b) that ultimately re-entrain water back into the reef-lagoon system. Therefore, although larger waves drive a stronger seaward flow out the channel (Figure 7a), which was also observed at the field site (r^2 = 0.89 between offshore waves and seaward flow velocities) and other reef sites [e.g. *Lowe et al.*, 2009], larger waves also enhance flow re-entrainment.

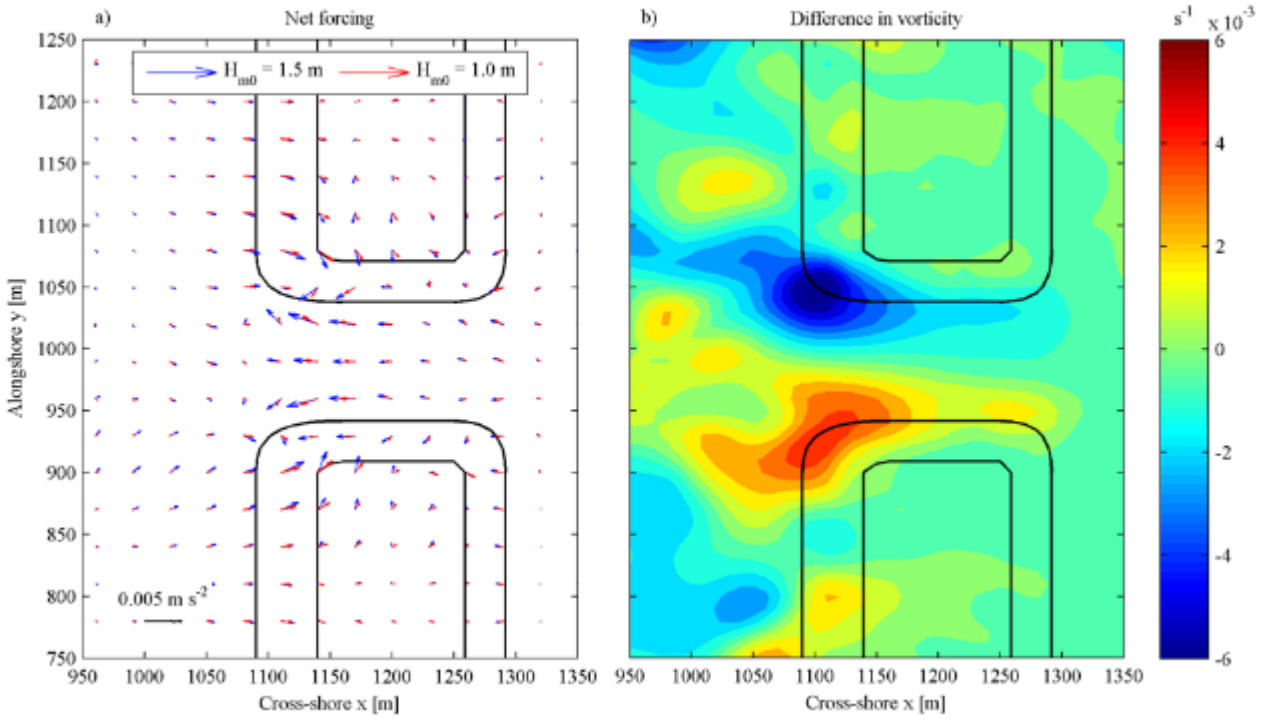

Figure 9. a) Modeled net forcing as the sum of the pressure gradient and wave forcing for a

514 simulation during small waves (H_{m0} = 1.0 m, b = 24%, red arrows) and the default case
515 (H_{m0} = 1.5 m, b = 38%, blue arrows). b) Difference in vertical vorticity between the two
516 simulations.

517

518 The increase of drifter re-entrainment with increasing wave height causes the exit rate
519 E_2 to decrease, which is consistent with field observations and modeling studies on rip-
520 channeled beaches [*Castelle et al.*, 2014; *Scott et al.*, 2014]. These studies have linked the
521 decrease in exit rate to: (1) increased onshore flow over the sand bars, which transports
522 drifters back towards shore [*Scott et al.*, 2014], and to (2) wider surf zones [*Castelle et al.*,
523 2014; *Reniers et al.*, 2009]. However, the surf zone width depends largely on the forereef
524 slope and varies less on steep forereefs. Here, we attribute the increased flow- re-entrainment
525 to the stronger onshore mass flux over the reef. An increase of re-entrainment with larger
526 waves implies that large storm waves may be increasingly less efficient in flushing costal reef
527 systems.

528 5.1.2 Alongshore current

529 In the presence of an inner-shelf alongshore current, the offshore current in the
530 channel is redirected towards the downdrift direction (Figure 10a). The cross-shore current
531 locally blocks the alongshore current resulting in a local increase in the water level updrift of
532 the channel and conversely a local decrease in the water level downdrift of the channel
533 (Figure 10). The modified pressure gradient, and thus the net forcing, are redirected towards
534 the downstream reef (Figure 10). This allows water to be transported towards the reef and
535 then back shoreward by the wave-driven cross-reef flow such that the re-entrainment b
536 increases and the exit rate E_2 decreases. This is consistent with the field observations at
537 Garden Island where drifters returned via the reef to the north of the channel when the

538 alongshore current outside the reef was directed northward. *Herdman* [2012] observed similar
539 dynamics at a large-scale coral reef where it was found that more drifters returned over a
540 downdrift reef in the presence of an increasing alongshore current. Similar observations have
541 been made on rip-channeled beaches where drifter re-entrainment increased in the presence
542 of alongshore currents associated with tidal flows [*Winter et al.*, 2014].

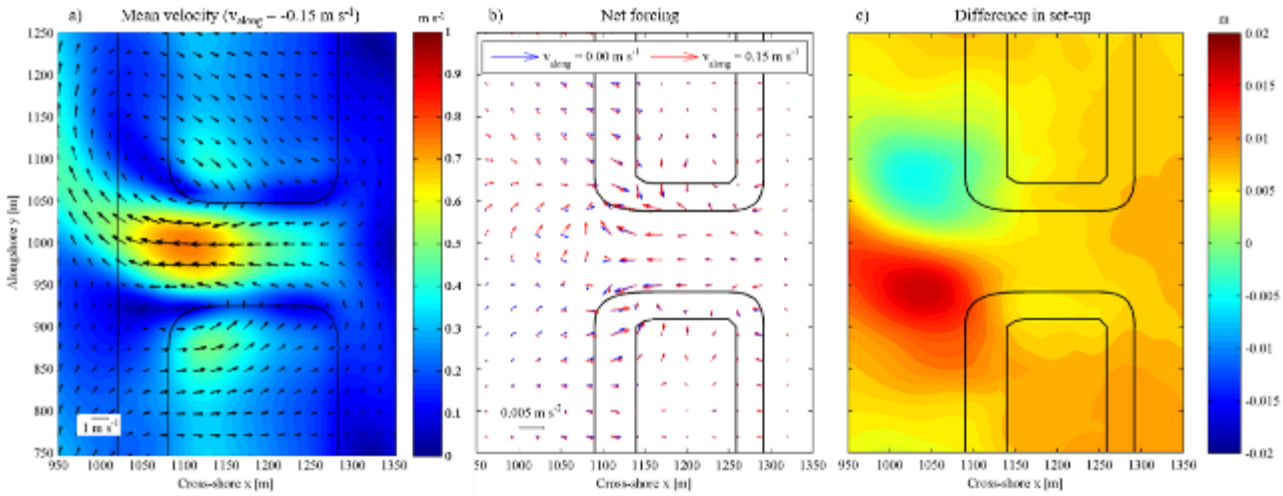

543 Figure 10. a) Mean velocity field for a simulation with a strong alongshore current
544 (v_0 = 0.15 ms^{-1}). b) Net forcing as the sum of the pressure gradient and wave forcing for a
545 simulation with strong alongshore current (v_0 = 0.15 ms^{-1}, b = 62%, red arrows) compared to
546 the default case (without alongshore current, b = 38%, blue arrows). c) Setup difference
547 between those simulations (red colors indicate greater setup in the simulation with strong
548 alongshore current).

549 5.1.3 Channel spacing

550 As the channel spacing increases, the ratio of channel width to alongshore reef width
551 decreases. To balance the volume of water flowing across the reef into the lagoon with the
552 volume of water flowing out through the channel, the seaward velocity in the channel
553 increases for larger channel spacing while the maximum onshore velocity over the reef

554 decreases (Figure 7c). Hence, water is advected further offshore rather than back towards the
555 reef. Drifter retention also decreases with increasing channel spacing on rip-channeled
556 beaches [*Castelle et al.*, 2014]. However, this study shows that this effect weakens with
557 larger channel spacing until a limit is reached where re-entrainment becomes approximately
558 constant (i.e. in larger-scale reef systems, re-entrainment becomes insensitive to the channel
559 spacing). Within the parameter space that we tested, this limit was ~500 m. Our results are
560 consistent with observations of less re-entrainment in large reef systems at Moorea, where
561 reef channels are 4 to 5 km apart and re-entrainment was less than 50% [*Herdman*, 2012].
562 Thus, small-scale reef systems appear to promote large re-entrainment rates.

563 5.2 A predictor for re-entrainment and its implications for flushing times

564 Based on the sensitivity of re-entrainment *b* to the tested reef geometry and
565 hydrodynamic parameters, we define a re-entrainment predictor variable *R* as:

$$R = \frac{H_{m0}}{h_{reef}} \frac{W_c}{\lambda} \tag{10}$$

566 Here the ratio of the offshore significant wave height to the water depth over the reef
567 (H_{m0}/h_{reef}) provides an indication of the intensity of wave dissipation on the reef; whereas
568 the ratio of the channel width to the channel spacing (W_c/λ) provides a measure for the
569 relative cross-sectional areas available for onshore and offshore mass transport. Both of these
570 ratios affect the balance between onshore flow velocity over the reef and offshore flow
571 velocity inside the channel. Stronger onshore flow over the reef favors drifter-re-entrainment
572 and stronger offshore flow transports drifters further offshore from where they are less likely
573 to be re-entrained. The alongshore current is considered separately because the re-
574 entrainment mechanism is fundamentally different (see section 5.1). An alongshore current
575 does not affect the cross-shore flow velocities but enhances flow re-entrainment because it

transports drifters towards an area of onshore flow.

We found that the exit rate E_2 decreases with R (r^2 = 0.70 in the absence of alongshore currents) following a negative reciprocal function while re-entrainment (b) increases with increasing values of R and plateaus with high values of R following a positive reciprocal function. In the absence of an alongshore current, b and the reciprocal of parameter R are correlated (r^2 = 0.73). With increasing alongshore current outside the reef the correlation between R and b reduces, i.e. when the current outside the reef is 0.15 m s^{-1}, the correlation coefficient drops to r^2 = 0.25 and re-entrainment is consistently higher across all values of R (Figure 11). The alongshore current outside the reef then dominates the re-entrainment process. For large values of R (>0.4), re-entrainment is less sensitive to the alongshore current outside the reef and the re-entrainment rates converge for all tested alongshore current magnitudes. To summarize, R and the alongshore current both increase re-entrainment, but when the alongshore current is strong it reduces the sensitivity to variations of R and vice versa.

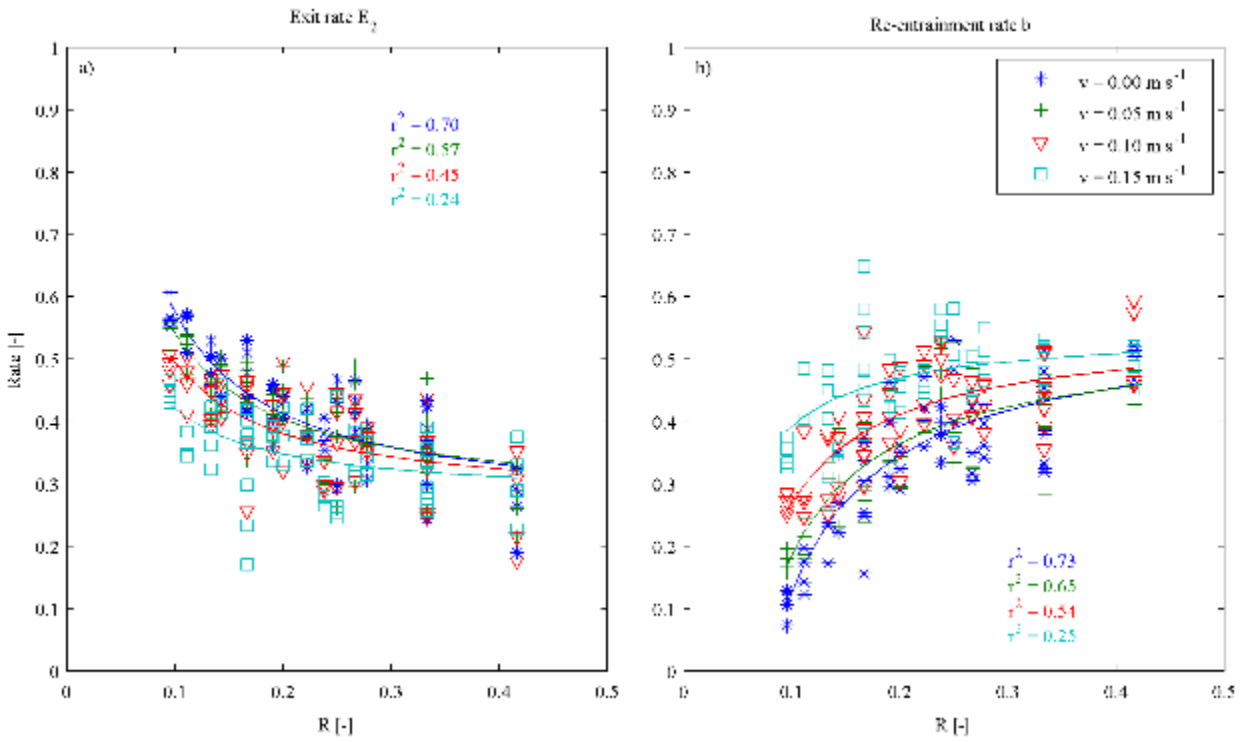

Figure 11. Exit rate E_2 (a) and re-entrainment b (b) versus the re-entrainment prediction parameter R for all simulations. The different marker colors denote variable alongshore currents outside the reef.

590

591 To demonstrate the implications of the large variability in re-entrainment (b) for reef
592 flushing times, we calculated the flushing time with re-entrainment (Eq. (2)) and without re-
593 entrainment (Eq. (1)). In many simulations, the inclusion of b in the estimate substantially
594 increased the flushing time compared to an estimate without re-entrainment: for 58% of the
595 simulations the flushing time increased by more than a factor of 1.5 and in 17% of the
596 simulations by more than two. The largest increase (greater than three times) was observed
597 for the simulations with large R (a combination of short channel spacing λ = 300 m and wave
598 heights of H_{m0} > 2 m) and strong alongshore currents. In contrast, there was little difference
599 between the two flushing times in simulations with small R (channel spacing λ > 500 m and
600 H_{m0} = 1 m) and no alongshore current.

6 Conclusions

This study examined the processes responsible for re-entrainment in wave-dominated reef systems. Drifter observations in a wave-dominated rocky limestone reef in southwestern Australia illustrated two distinct flow patterns of either complete drifter ejection or drifter re-entrainment. These observations motivated an idealized numerical study that investigated the effect of reef channel spacing and reef roughness along with offshore wave height and alongshore currents on flow re-entrainment. The model demonstrated that large waves and strong alongshore currents outside the reef enhance flow re-entrainment. The model results further showed that large reef channel spacing reduces flow re-entrainment, while the reef roughness had no effect. A single re-entrainment prediction parameter R is proposed, which incorporates the effect of wave forcing and reef geometry. For large values of R (i.e. large offshore wave height and small channel spacing) and strong alongshore currents outside the reef flow re-entrainment is important to consider in reef flushing time estimates. Large wave heights can dominate the re-entrainment mechanism and reduce the positive effect of an alongshore current outside the reef and vice versa.

The present study demonstrates that re-entrainment rates can be large and highly variable among reefs, and thus should be included when assessing flushing times and material exchange of reef systems with the surrounding ocean. High re-entrainment rates may limit the ability of a reef to exchange material with both the surrounding ocean and other reef systems, and thus further emphasizes the need to accurately quantify flow re-entrainment to make robust estimates of, for example, larval dispersal, reef connectivity [*Cowen et al.*, 2000; *Teske et al.*, 2016] and reef water quality [*Falter et al.*, 2013; *Lowe and Falter*, 2015]. Flow re-entrainment is generally important for reefs that are frequently intercepted by channels and reefs that are exposed to large waves and strong alongshore currents outside the reef.

Acknowledgements

We are grateful to Andrew Pomeroy, Mike Cuttler, Anton Kuret, Laura Segura and Mark Buckley for assistance with the instrument deployment and recovery. Funding for this project was provided by an ARC Future Fellowship (FT110100201) and ARC Discovery Project (DP140102026) to RJL. This work was undertaken by GW as part of a PhD at The University of Western Australia and was funded by an International Postgraduate Research Scholarship, an Australian Postgraduate Award and an EA and CH Jenkins scholarship. GW also acknowledges a Sue Baker Convocation Travel Award, which allowed her to visit the University of Bordeaux, where a large part of this manuscript was developed. BC was financially supported by projects DECA (INSU/EC2CO-DRIL) and CHIPO (grant number ANR-14-ASTR-0004-01) supported by the Agence Nationale de la Recherche (ANR). Funding for RM was provided by the "Hydro- and morphodynamics during extreme events" research program of Deltares. The numerical modeling work was supported by resources provided by The Pawsey Supercomputing Centre with funding from the Australian Government and the Government of Western Australia. The data are available under http://doi.org/10.5281/zenodo.1292064.

Appendix A. Momentum equations

Output from the idealized XBeach simulations was used to assess the relative importance of the terms of the steady ($d/dt = 0$) depth and time (wave) averaged momentum balances in cross (x)- and alongshore (y) direction including the wave (radiation stress) forcing, F_x and F_y, as source term and pressure gradients, advection, turbulent mixing, and bottom shear stress, as sink terms:

$$\frac{F_x}{\rho} - g(\eta + h)\frac{\partial \eta}{\partial x} - (\eta + h)\left(u\frac{\partial u}{\partial x} + v\frac{\partial u}{\partial y}\right) - \upsilon_H(\eta + h)\left(\frac{\partial^2 u}{\partial x^2} + \frac{\partial^2 u}{\partial y^2}\right) - \frac{\tau_x^b}{\rho} = 0 \tag{A1}$$

$$\frac{F_y}{\rho} - g(\eta + h)\frac{\partial \eta}{\partial y} - (\eta + h)\left(u\frac{\partial v}{\partial x} + v\frac{\partial v}{\partial y}\right) - \upsilon_H(\eta + h)\left(\frac{\partial^2 v}{\partial x^2} + \frac{\partial^2 v}{\partial y^2}\right) - \frac{\tau_y^b}{\rho} = 0 \tag{A2}$$

where ρ is the water density, η is setup, h the still water depth, u and v are the cross- and alongshore velocities, υ_H the horizontal viscosity and τ_x^b and τ_y^b are the bottom shear stresses in cross- and alongshore direction. The wave forcing is calculated from the radiation stress gradients S_{ij} as follows:

$$F_x = -\left(\frac{\partial(S_{xx} + S_{xx,roller})}{\partial x} + \frac{\partial(S_{xy} + S_{xy,roller})}{\partial y}\right) \tag{A3}$$

$$F_y = -\left(\frac{\partial(S_{yx} + S_{yx,roller})}{\partial x} + \frac{\partial(S_{yy} + S_{yy,roller})}{\partial y}\right) \tag{A4}$$

652 **References**

653 Austin, M. J., T. M. Scott, J. W. Brown, J. A. Brown, J. H. MacMahan, G. Masselink, and P.
654 Russell (2010), Temporal observations of rip current circulation on a macro-tidal
655 beach, *Continental Shelf Research*, *30*, 1149-1165, doi:10.1016/j.csr.2010.03.005.
656 Barnard, P. L., J. E. Hansen, and L. H. Erikson (2012), Synthesis study of an erosion hot spot,
657 Ocean Beach, California, *Journal of Coastal Research*, *28*(4), 903-922,
658 doi:10.2112/JCOASTRES-D-11-00212.1.
659 Black, K. P., S. L. Gay, and J. C. Andrews (1990), Residence times of neutrally-buoyant
660 matter such as larvae, sewage or nutrients on coral reefs, *Coral Reefs*, *9*(3), 105-114,
661 doi:10.1007/bf00258221.
662 Bosserelle, C., Pattiaratchi, C., & Haigh, I. (2012), Inter-annual variability and longer-term
663 changes in the wave climate of Western Australia between 1970 and 2009. *Ocean*
664 *Dynamics*, *62*(1), 63–76. https://doi.org/10.1007/s10236-011-0487-3
665 Brown, J. A., J. H. MacMahan, A. J. H. M. Reniers, and E. B. Thornton (2015), Field
666 Observations of Surf Zone–Inner Shelf Exchange on a Rip-Channeled Beach, *Journal*
667 *of Physical Oceanography*, *45*(9), 2339-2355, doi:10.1175/JPO-D-14-0118.1.
668 Buckley, M. L., R. J. Lowe, J. E. Hansen, and A. R. Van Dongeren (2016), Wave Setup over
669 a Fringing Reef with Large Bottom Roughness, *Journal of Physical Oceanography*,
670 *46*(8), 2317-2333, doi:10.1175/JPO-D-15-0148.1.
671 Bureau of Meterology Commonwealth of Australia (2014), Climate statistics for Australian
672 locations, edited by BOM, Bureau of Meterology, Commonwealth of Australia,
673 Melbourne.
674 Castelle, B., and G. Coco (2013), Surf zone flushing on embayed beaches, *Geophysical*
675 *Research Letters*, *40*(10), 2206-2210, doi:10.1002/grl.50485.
676 Castelle, B., A. J. H. M. Reniers, and J. H. MacMahan (2014), Bathymetric control of surf

zone retention on a rip-channelled beach, *Ocean Dynamics*, *64*(8), 1221-1231, doi:10.1007/s10236-014-0747-0.

Castelle, B., T. Scott, R. W. Brander, and R. J. McCarroll (2016), Rip current types, circulation and hazard, *Earth-Science Reviews*, *163*, 1-21, doi:10.1016/j.earscirev.2016.09.008.

Coronado, C., J. Candela, R. Iglesias-Prieto, J. Sheinbaum, M. López, and F. J. Ocampo-Torres (2007), On the circulation in the Puerto Morelos fringing reef lagoon, *Coral Reefs*, *26*(1), 149-163, doi:10.1007/s00338-006-0175-9.

Cowen, R. K., K. M. M. Lwiza, S. Sponaugle, C. B. Paris, and D. B. Olson (2000), Connectivity of Marine Populations: Open or Closed?, *Science*, *287*(5454), 857, doi:10.1126/science.287.5454.857

Dalrymple, R. A., J. H. MacMahan, A. J. H. M. Reniers, and V. Nelko (2011), Rip Currents, *Annual Review of Fluid Mechanics*, *43*(1), 551-581, doi:10.1146/annurev-fluid-122109-160733.

Dean, R. G. (1977), Equilibrium beach profiles: US Atlantic and Gulf coasts. *Rep.*, University of Delaware.

Department of Transport Western Australia (2009), Two Rocks to Cape Naturaliste Bathymetry and Seabed LiDAR Survey, edited by DoT, Department of Transport, Western Australia, Perth.

Falter, J. L., M. J. Atkinson, and M. A. Merrifield (2004), Mass-transfer limitation of nutrient uptake by a wave-dominated reef flat community, *Limnology and Oceanography*, *49*(5), 1820-1831, doi:10.4319/lo.2004.49.5.1820.

Falter, J. L., R. J. Lowe, Z. Zhang, and M. McCulloch (2013), Physical and Biological Controls on the Carbonate Chemistry of Coral Reef Waters: Effects of Metabolism, Wave Forcing, Sea Level, and Geomorphology, *PLoS ONE*, *8*(1), e53303,

doi:10.1371/journal.pone.0053303.

Feddersen, F., R. T. Guza, S. Elgar, and T. H. C. Herbers (1998), Alongshore momentum balances in the nearshore, *Journal of Geophysical Research: Oceans*, *103*(C8), 15667-15676, doi:10.1029/98jc01270.

Feddersen, F., R. T. Guza, S. Elgar, and T. H. C. Herbers (2000), Velocity moments in alongshore bottom stress parameterizations, *Journal of Geophysical Research: Oceans*, *105*(C4), 8673-8686, doi:10.1029/2000jc900022.

Fischer, H. B., J. E. List, C. R. Koh, J. Imberger, and N. H. Brooks (1979), *Mixing in Inland and Coastal Waters*, Academic Press, New York.

Gersbach, G. H., C. B. Pattiaratchi, G. N. Ivey, and G. R. Cresswell (1999), Upwelling on the south-west coast of Australia—source of the Capes Current?, *Continental Shelf Research*, *19*(3), 363-400, doi:10.1016/S0278-4343(98)00088-0.

Geyer, W. R., & MacCready, P. (2014), The Estuarine Circulation. Annual Review of Fluid Mechanics, 46(1), 175–197, doi:10.1146/annurev-fluid-010313-141302

González, M., R. Medina, and M. A. Losada (1999), Equilibrium beach profile model for perched beaches, *Coastal Engineering*, *36*(4), 343-357, doi:10.1016/S0378-3839(99)00018-6.

Hally-Rosendahl, K., F. Feddersen, and R. T. Guza (2014), Cross-shore tracer exchange between the surfzone and inner-shelf, *Journal of Geophysical Research: Oceans*, *119*(7), 4367-4388, doi:10.1002/2013JC009722.

Hench, J., L., J. J. Leichter, and S. G. Monismith (2008), Episodic circulation and exchange in a wave-driven coral reef and lagoon system, *Limnol. Oceanogr.*, *53*(6), 2681-2694, doi:10.4319/lo.2008.53.6.2681.

Herdman, L. M. M. (2012), Circulation, Residence Time and Retention in a Tropical Coral Reef, Stanford University.

727 Herdman, L. M. M., J. L. Hench, and S. G. Monismith (2015), Heat balances and thermally
728 driven lagoon-ocean exchanges on a tropical coral reef system (Moorea, French
729 Polynesia), *Journal of Geophysical Research: Oceans*, *120*, 1233-1252,
730 doi:10.1002/2014JC010145.
731 Hoeke, R., C. D. Storlazzi, and P. Ridd (2011), Hydrodynamics of a bathymetrically complex
732 fringing coral reef embayment: Wave climate, in situ observations, and wave
733 prediction, *Journal of Geophysical Research: Oceans*, *116*(C4), C04018,
734 doi:10.1029/2010JC006170.
735 Kench, S. P. (1998), Physical processes in an Indian Ocean atoll, *Coral Reefs*, *17*(2), 155-
736 168, doi:10.1007/s003380050110.
737 Kraines, B. S., A. Suzuki, T. Yanagi, M. Isobe, X. Guo, and H. Komiyama (1999), Rapid
738 water exchange between the lagoon and the open ocean at Majuro Atoll due to wind,
739 waves and tide, *Journal of Geophysical Research*, *104*(C7), 15635-15653,
740 doi:10.1029/1999JC900065.
741 Large, W. G., and S. Pond (1981), Open Ocean Momentum Flux Measurements in Moderate
742 to Strong Winds, *Journal of Physical Oceanography*, *11*(3), 324-336,
743 doi:10.1175/1520-0485(1981)011<0324:OOMFMI>2.0.CO;2.
744 Longuet-Higgins, M. S. (1962), Radiation stress and mass transport in gravity waves, with
745 application to 'surf beats', *Journal of Fluid Mechanics*, *13*(04), 481- 504,
746 doi:10.1017/S0022112062000877.
747 Lowe, R. J., and J. L. Falter (2015), Oceanic Forcing of Coral Reefs, *Annual Review of*
748 *Marine Science*, *7*(1), 43-66, doi:10.1146/annurev-marine-010814-015834.
749 Lowe, R. J., J. L. Falter, S. G. Monismith, and M. J. Atkinson (2009), Wave-Driven
750 Circulation of a Coastal Reef–Lagoon System, *Journal of Physical Oceanography*,
751 *39*(4), 873-893, doi:10.1175/2008JPO3958.1.

752 Lowe, R. J., C. Hart, and C. B. Pattiaratchi (2010), Morphological constraints to wave-driven
753 circulation in coastal reef-lagoon systems: A numerical study, *Journal of Geophysical*
754 *Research: Oceans*, *115*(C9), C09021, doi:10.1029/2009JC005753.
755 Lugo-Fernández, A., K. J. P. Deslarzes, J. M. Price, G. S. Boland, and M. V. Morin (2001),
756 Inferring probable dispersal of Flower Garden Banks Coral Larvae (Gulf of Mexico)
757 using observed and simulated drifter trajectories, *Continental Shelf Research*, *21*(1),
758 47-67, doi:10.1016/S0278-4343(00)00072-8.
759 MacMahan, J. H. (2001), Hydrographic surveying from a personal watercraft, *Journal of*
760 *Surveying Engineering*, *127*(1), 12-24, doi:10.1061/(ASCE)0733-
761 9453(2001)127:1(12)#sthash.boohLR0J.dpuf.
762 MacMahan, J. H., et al. (2010a), Mean Lagrangian flow behavior on an open coast rip-
763 channeled beach: A new perspective, *Marine Geology*, *268*(1-4), 1-15,
764 doi:10.1016/j.margeo.2009.09.011.
765 MacMahan, J. H., A. J. H. M. Reniers, and E. B. Thornton (2010b), Vortical surf zone
766 velocity fluctuations with 0(10) min period, *Journal of Geophysical Research:*
767 *Oceans*, *115*(C6), C06007, doi:10.1029/2009JC005383.
768 McCarroll, R. J., R. W. Brander, T. Scott, and B. Castelle (2018), Bathymetric controls on
769 rotational surfzone currents, *Journal of Geophysical Research: Earth Surface*, *123*(6),
770 1295-1316.
771 McCarroll, R. J., R. W. Brander, I. L. Turner, H. E. Power, and T. R. Mortlock (2014),
772 Lagrangian observations of circulation on an embayed beach with headland rip
773 currents, *Marine Geology*, *355*, 173-188, doi:10.1016/j.margeo.2014.05.020.
774 Monismith, S. G. (2013), Flow through a rough, shallow reef, *Coral Reefs*, *33*(1), 99-104,
775 doi:10.1007/s00338-013-1107-0.
776 Monsen, N. E., J. E. Cloern, L. V. Lucas, and S. G. Monismith (2002), A comment on the use

of flushing time, residence time, and age as transport time scales, *Limnology and Oceanography, 47*(5), 1545-1553, doi:10.4319/lo.2002.47.5.1545.

Morgan, S. G., A. L. Shanks, A. G. Fujimura, A. J. H. M. Reniers, J. MacMahan, C. D. Griesemer, M. Jarvis, and J. Brown (2016), Surfzone hydrodynamics as a key determinant of spatial variation in rocky intertidal communities, *Proceedings of the Royal Society B: Biological Sciences, 283*(1840), doi:10.1098/rspb.2016.1017.

Reidenbach, M. A., S. G. Monismith, J. R. Koseff, G. Yahel, and A. Genin (2006), Boundary layer turbulence and flow structure over a fringing coral reef, *Limnology and Oceanography, 51*(5), 1956-1968, doi:10.4319/lo.2006.51.5.1956.

Reniers, A. J. H. M., J. H. MacMahan, E. B. Thornton, T. P. Stanton, M. Henriquez, J. W. Brown, J. A. Brown, and E. Gallagher (2009), Surf zone surface retention on a rip-channeled beach, *Journal of Geophysical Research, 114*(C10), C10010, doi:10.1029/2008jc005153.

Roelvink, J. A. (1993), Dissipation in random wave groups incident on a beach, *Coastal Engineering, 19*(1-2), 127-150, doi:10.1016/0378-3839(93)90021-Y.

Roelvink, J. A., A. J. H. M. Reniers, A. R. van Dongeren, J. S. M. van Thiel de Vries, R. T. McCall, and J. Lescinski (2009), Modelling storm impacts on beaches, dunes and barrier islands, *Coastal Engineering, 56*(11-12), 1133-1152, doi:10.1016/j.coastaleng.2009.08.006.

Rosman, J. H., and J. L. Hench (2011), A framework for understanding drag parameterizations for coral reefs, *Journal of Geophysical Research: Oceans, 116*(C8), C08025, doi:10.1029/2010JC006892.

Ruessink, B. G., J. R. Miles, F. Feddersen, R. T. Guza, and S. Elgar (2001), Modeling the alongshore current on barred beaches, *Journal of Geophysical Research, 106*, 22451-22464, doi:10.1029/2000JC000766.

802 Ruiz-Montoya, L., and R. J. Lowe (2014), Summer circulation dynamics within the Perth
803 coastal waters of southwestern Australia, *Continental Shelf Research*, *77*(0), 81-95,
804 doi:10.1016/j.csr.2014.01.022.
805 Sanford, L. P., W. C. Boicourt, and S. R. Rives (1992), Model for Estimating Tidal Flushing
806 of Small Embayments, *Journal of Waterway, Port, Coastal, and Ocean Engineering*,
807 *118*(6), 635-654, doi:10.1061/(ASCE)0733-950X(1992)118:6(635).
808 Schmidt, W. E., B. T. Woodward, K. S. Millikan, R. T. Guza, B. Raubenheimer, and S. Elgar
809 (2003), A GPS-tracked surf zone drifter, *Journal of Atmospheric and Oceanic*
810 *Technology*, *20* (Compendex), 1069-1075, doi:10.1175/1460.1.
811 Scott, T., G. Masselink, M. J. Austin, and P. Russell (2014), Controls on macrotidal rip
812 current circulation and hazard, *Geomorphology*, *214*(0), 198-215,
813 doi:10.1016/j.geomorph.2014.02.005.
814 Smagorinsky, J. (1963), General circulation experiments with the primitive equations,
815 *Monthly Weather Review*, *91*(3), 99-164, doi:10.1175/1520-
816 0493(1963)091<0099:gcewtp>2.3.co;2.
817 Spydell, M. S. (2016), The Suppression of Surfzone Cross-shore Mixing by Alongshore
818 Currents, *Geophysical Research Letters*, *43*, doi:10.1002/2016GL070626.
819 Spydell, M. S., F. Feddersen, R. T. Guza, and W. E. Schmidt (2007), Observing surf-zone
820 dispersion with drifters, *Journal of Physical Oceanography*, *37* (Compendex), 2920-
821 2939, doi:10.1175/2007JPO3580.1.
822 Storlazzi, C. D., A. S. Ogston, M. H. Bothner, M. E. Field, and M. K. Presto (2004), Wave-
823 and tidally-driven flow and sediment flux across a fringing coral reef: Southern
824 Molokai, Hawaii, *Continental Shelf Research*, *24*(12), 1397-1419,
825 doi:10.1016/j.csr.2004.02.010.
826 Svendsen, I. A., K. A. Haas, and Q. Zhao (2000), Analysis of Rip Current Systems, in *29th*

827 *International Conference on Coastal Engineering*, edited by B. L. Edge, pp. 1127-
828 1140, American Society of Civil Engineers, Sydney.
829 Symonds, G., K. P. Black, and I. R. Young (1995), Wave-driven flow over shallow reefs,
830 *Journal of Geophysical Research: Oceans*, *100*(C2), 2639-2648,
831 doi:10.1029/94JC02736.
832 Symonds, G., D. A. Huntley, and A. J. Bowen (1982), Two-dimensional surf beat: Long
833 wave generation by a time-varying breakpoint, *Journal of Geophysical Research*,
834 *87*(C1), 492-498, doi:10.1029/JC087iC01p00492.
835 Taebi, S., R. J. Lowe, C. B. Pattiaratchi, G. N. Ivey, and G. Symonds (2012), A numerical
836 study of the dynamics of the wave-driven circulation within a fringing reef system,
837 *Ocean Dynamics*, *62*(4), 585-602, doi:10.1007/s10236-011-0514-4.
838 Taebi, S., R. J. Lowe, C. B. Pattiaratchi, G. N. Ivey, G. Symonds, and R. Brinkman (2011),
839 Nearshore circulation in a tropical fringing reef system, *Journal of Geophysical*
840 *Research: Oceans*, *116*(C2), 2156-2202, doi:10.1029/2010JC006439.
841 Tartinville, B., E. Deleersnijder, and J. Rancher (1997), The water residence time in the
842 Mururoa atoll lagoon: sensitivity analysis of a three-dimensional model, *Coral Reefs*,
843 *16*(3), 193-203, doi:10.1007/s003380050074.
844 Teske, P. R., J. Sandoval-Castillo, E. van Sebille, J. Waters, and L. B. Beheregaray (2016),
845 Oceanography promotes self-recruitment in a planktonic larval disperser, *Scientific*
846 *Reports*, *6*, 34205, doi:10.1038/srep34205.
847 van Dongeren, A. R., R. J. Lowe, A. W. M. Pomeroy, D. M. Trang, J. A. Roelvink, G.
848 Symonds, and R. Ranasinghe (2013), Numerical modeling of low-frequency wave
849 dynamics over a fringing coral reef, *Coastal Engineering*, *73*(0), 178-190,
850 doi:10.1016/j.coastaleng.2012.11.004.
851 Vetter, O., J. M. Becker, M. A. Merrifield, A. C. Pequignet, J. Aucan, S. J. Boc, and C. E.

852 Pollock (2010), Wave setup over a Pacific Island fringing reef, *Journal of*
853 *Geophysical Research: Oceans, 115*(12), C12066,, doi:10.1029/2010JC006455.
854 Willmott, C. J., S. G. Ackleson, R. E. Davis, J. J. Feddema, K. M. Klink, D. R. Legates, J.
855 O'Donnell, and C. M. Rowe (1985), Statistics for the Evaluation and Comparison of
856 Models, *Journal of Geophysical Research*, *90*(C5), 8995-9005,
857 doi:10.1029/JC090iC05p08995.
858 Winter, G., A. R. van Dongeren, M. A. de Schipper, and J. S. M. van Thiel de Vries (2014),
859 Rip currents under obliquely incident wind waves and tidal longshore currents,
860 *Coastal Engineering*, *89*, 106-119, doi:10.1016/j.coastaleng.2014.04.001.
861 Zaker, N. H., J. Imberger, and C. Pattiaratchi (2007), Dynamics of the Coastal Boundary
862 Layer off Perth, Western Australia, *Journal of Coastal Research*, *23*(5), 1112-1130,
863 doi:10.2112/04-0374.1.
864 Zhang, Z., J. Falter, R. Lowe, and G. Ivey (2012), The combined influence of hydrodynamic
865 forcing and calcification on the spatial distribution of alkalinity in a coral reef system,
866 *Journal of Geophysical Research: Oceans*, *117*(C4), doi:10.1029/2011jc007603.
867 Zhang, Z., J. Falter, R. Lowe, G. Ivey, and M. McCulloch (2013), Atmospheric forcing
868 intensifies the effects of regional ocean warming on reef-scale temperature anomalies
869 during a coral bleaching event, *Journal of Geophysical Research: Oceans*, *118*(9),
870 4600-4616, doi:10.1002/jgrc.20338.
871